Journal of Applied Physics

Toward single-layer Janus crystals: Off-balance materials from synthesis to nanotechnology applications

Cite as: J. Appl. Phys. **129**, 160902 (2021); https://doi.org/10.1063/5.0041054
Submitted: 18 December 2020 • Accepted: 06 April 2021 • Published Online: 23 April 2021

H. Esra Oguzturk, Yigit Sozen, Cansu Akyol, et al.

Journal of Applied Physics PERSPECTIVE scitation.org/journal/jap

Toward single-layer Janus crystals: Off-balance materials from synthesis to nanotechnology applications

Cite as: J. Appl. Phys. **129**, 160902 (2021); doi: 10.1063/5.0041054
Submitted: 18 December 2020 · Accepted: 6 April 2021 ·
Published Online: 23 April 2021

H. Esra Oguzturk,[1] Yigit Sozen,[1] Cansu Akyol,[1] Dilce Ozkendir Inanc,[1] Umit Hakan Yildiz,[2] and Hasan Sahin[1,a)]

AFFILIATIONS

[1]Department of Photonics, Izmir Institute of Technology, 35430 Urla, Izmir, Turkey
[2]Department of Chemistry, Izmir Institute of Technology, 35430 Urla, Izmir, Turkey

[a)]**Author to whom correspondence should be addressed:** hasansahin@iyte.edu.tr

ABSTRACT

The existence of things is directly related to their structural symmetry in a broad framework ranging from atoms to crystalline materials and from simple cells to complex organisms like humans. However, structural imbalance that occurs through natural or artificial means can provide completely different advantages. Molecules, crystals, and complex structures with structural imbalance constitute the family of Janus-type materials. This perspective provides a comprehensive discussion on the synthesis techniques of Janus-type materials, their use in fields from biology to materials science, and very recent studies on the family of 2D ultrathin graphene-like structures. We believe that, thanks to the advances in experimental techniques, the few-atom-sized off-balanced materials will be indispensable parts of the nanotechnology products that soon will be used in our daily lives.

I. TILTING THE BALANCE AT NANOSCALE

Asymmetric structures have been playing pivotal roles in physical and chemical properties of simple solid or complex living systems. The hierarchical organization driven by simple asymmetric structure of molecules has pushed chemists to think out of the box by revolutionizing the classical synthetic modalities to obtain novel materials.[1,2] The Janus-type materials have emerged as an extraordinary outcome of the unconventional fabrication strategies and they have provided new dimensions and numerous possibilities for obtaining optical probes (modulated optical probes), anisotropic optical probes for optical traps, reconfigurable materials (electronic paper), self-propelling particles, and biomedical applications like drug delivery, bioimaging, and biosensing.[1–3] Janus particles (JPs), named after the Roman god Janus and shown in Figs. 1(a) and 1(b),[4] were highlighted by de Gennes in his 1991 Nobel Prize lecture. The term "Janus" represents anisotropic structures with two incompatible constituents in the same body.[5,6] More specifically, the structures having shape-wise, composition-wise asymmetry and hybrid particles in which both shape- and composition-wise anisometry are seen, have been called Janus-type structures for three decades.

Polymeric, inorganic, organic–inorganic, and polymeric–inorganic materials are the most common materials preferred to obtain Janus-type structures.[7–9] Since the first report on Janus-type particles, several fabrication methodologies have been developed ranging from phase separation, immobilization, surface control nucleation, and growth to self-assembly, synthesis in microfluidics, and emulsion polymerization.[3] Preparation methods to obtain Janus materials and the potential application areas are directly related to each other. For instance, bichromal dipolar Janus-type particles enable to end up with electronic displays whereas toposelective functionalization of hemispheres with different chemical groups provides the ability of bifunctional carrying to the prepared Janus materials suitable for the applications like catalysis, sensing, and drug delivery.[10]

Nowadays, the research studies on Janus-type particles and materials have achieved certain advancement since their bulk production has been facilitated significantly [see Fig. 1(c)]. Unlike conventional colloids, Janus-type particles have enabled the

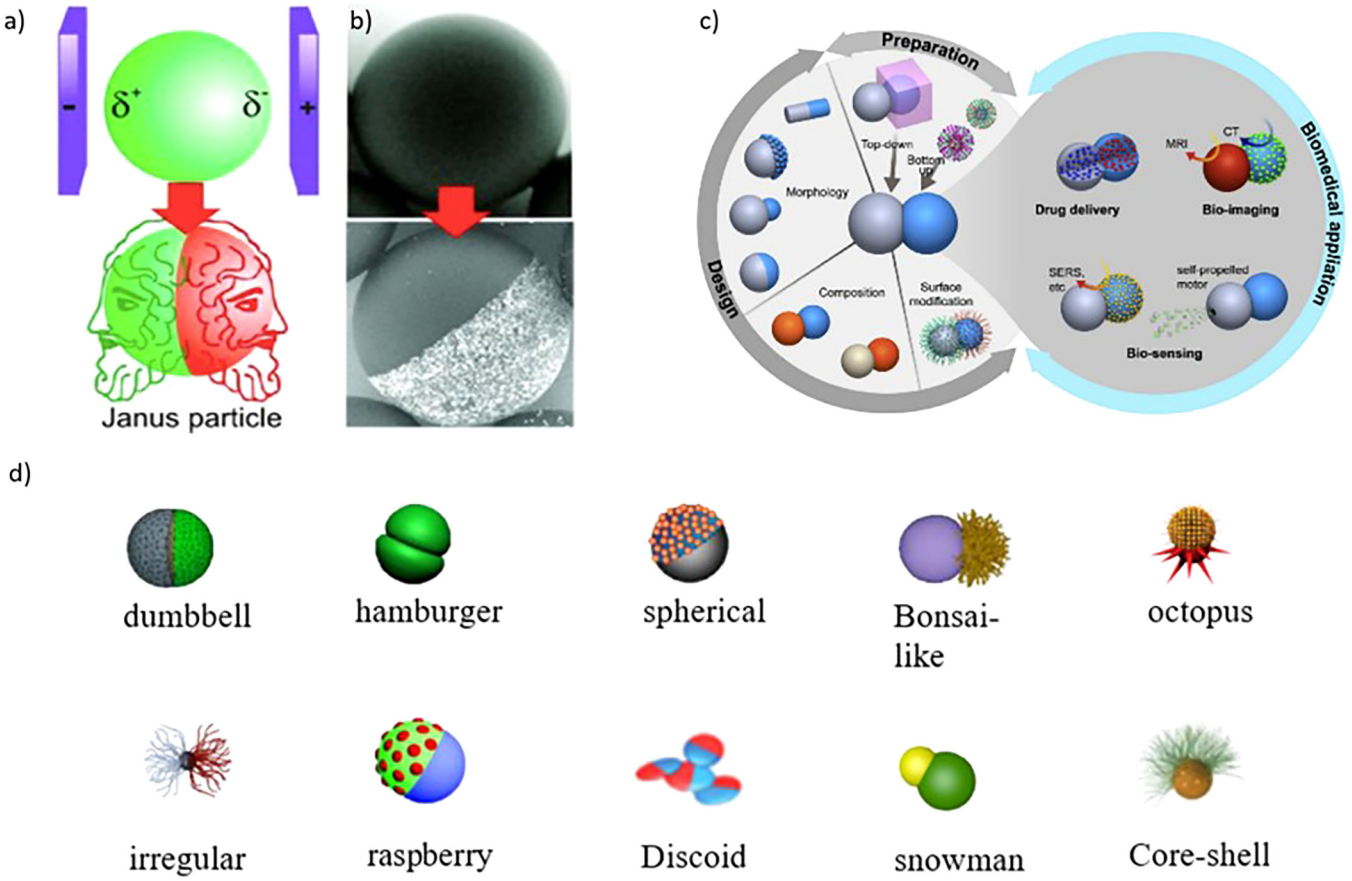

FIG. 1. (a) Principle of bipolar electrodeposition for Janus particles. This schematic representation represents the polarization of a conducting particle allowing the geometrical symmetry to be broken. (b) SEM images of glassy carbon before and after the bipolar electrodeposition process. Reproduced with permission from Loget *et al.*, Adv. Mater. **24**, 5111 (2012). Copyright 2012 Wiley-VCH. (c) Schematic representation of design, preparation, and biomedical application of Janus particles. (d) Typical Janus morphologies. Reproduced with permission from Su *et al.*, Mater. Today Bio. **4**, 100033 (2019). Copyright 2019 Elsevier.

responsiveness, triggered manipulation, and optical modulation that revolutionize classical colloidal systems. In particular, Janus materials lead to the programmable self-assembled super structures and periodic patterns enabling collective response to external stimuli. In contrast to the bulk materials, self-assembled super structures made of Janus-type building blocks have a promising potential to obtain tunable properties for macroscopic matter [see Fig. 1(d)].

In addition to the application areas mentioned above, the synthesis of Janus-type few-atom-thick-2D materials was achieved in the last decade. When the unique properties of graphene-like 2D materials are taken into consideration, it is obvious that ultrathin Janus-type crystals have a great potential for various nanotechnological applications. This perspective presents a comprehensive discussion starting with the chronological developments in chemistry and biology, which is followed by ultrathin Janus materials progressing.

II. CHEMICAL APPLICATIONS OF JANUS MATERIALS

As briefly mentioned in the introduction part, there are several ways in order to obtain a Janus system. The synthetic pathways differ based on the materials used, limitations of the procedures, and the desired application areas of the end product. There are three main methods commonly used for the preparation of Janus systems: Self-Assembly, Masking, and Phase Separation of a heterogeneous mixture.[11,12] In Self-Assembly based synthesis, an ABC type triblock copolymer is prepared via cross-linking of two deblock copolymers AB and BC, where A and C are incompatible with each other.[13] Masking is a technique for functionalizing half of a particle while the other half is entrapped with an immobilizing agent like wax. After functionalization of the particles, the immobilization agent is easily removed with organic solvents.[14] Lastly, Phase Separation is a method particularly used for biodegradable Janus particles and this method could be applied via microfluidics

or electrohydrodynamic co-jetting.[15–18] Microfluidics serve a system in which there are coordinatively working two channels with a parallel flowing stream and a stable interface. Janus geometry is ensured via UV radiation, heat, or chemical treatment applied to the system.[15] Electrohydrodynamic co-jetting type phase separation is based on electrospinning of two different polymers filled in separate channels. When the voltage applied to the system, the bipolar liquid is formed between the tip and the collector screen giving rise to Janus particles having different polymers at opposite hemispheres.[18]

Besides these three main methods, seeded polymerization, which enables to obtain Janus particles with dumbbell, acorn-like, and snowman-like morphologies;[14,19–21] and Pickering emulsion/emulsion solvent evaporation method, which is based on the evaporation of the solvent dissolving two incompatible polymers with the help of shear force,[14,22] are the methods commonly preferred for the preparation of Janus particles.

The interest increasing day by day on the 2D materials brought the necessity of the new aspects on the synthesis of 2D Janus systems and structures such as Janus nanosheets and Janus onions. Recently, the preparation of graphene-based amphiphilic Janus nanosheets via an improved masking method applied on graphene oxide by immobilization of the hydrogen bonding on the surfaces of starch microspheres was reported.[23] Another synthetic pathway to obtain amphiphilic Janus nanosheets was performed via an enhanced Pickering emulsion method: electrostatic attraction-induced high internal phase emulsion.[24] As another example of the recent preparation perspectives, Janus onions of block copolymers were prepared via interfacial phase separation with an unconventional strategy enabling to control the confined assembly of block copolymers.[25]

A. Sensors

There are numerous applications in the literature on the utilization of Janus materials in chemistry from sensor applications to environmentally friendly solutions. Many of these applications are either related or they lead the improvement of the incoming technologies. To begin with the electrochemical applications of Janus-type materials, it has been stated since three decades that they are promising materials to be used for the improvement of actuators, switches, valves, and power sources for nanoscale electronic, optical, magnetic, mechanical, and fluid dynamic devices.[26] There are plenty of examples in the literature on the electrochemical applications of Janus materials; however, it has to be mentioned that all these studies were launched after Fournier-Bidoz *et al.* reported self-powered synthetic barcoded bimetal nanorotor composed of nickel and gold for the decomposition of hydrogen peroxide.[27] In this study, nickel is catalyzing the decomposition of hydrogen peroxide leading to the motion of the nanorod. A year later, platinum-gold nanorod was presented,[28] in which Pt-Au nanorods were not only catalyzing the decomposition of hydrogen peroxide but also leading to the reduction of hydrogen peroxide into water. In this self-electrophoretic micromotor, decomposition of hydrogen peroxide takes place on the Pt end of the micromotor and the protons and the electrons formed by the decomposition reaction are then consumed by the Au end. The resulting ion flux activates the motion of the particle relative to the fluid.

Electrochemical applications are strongly interrelated with sensor applications as many of the mechanisms used for sensor applications are based on electrochemistry. There are plenty of research reported in the literature on the sensing ability of Janus materials for chemical and biological applications. The latter one will be discussed in Sec. III in detail. As the earliest chemical sensor application, Choi *et al.* reported a pioneering technique for the observation of the molecular interactions by using optical measurements of the rotations of nanoparticles by introducing thin gold film coated fluorescent polystyrene (PS) spheres as modulated optical nanoprobes (MOONs).[29] These gold half-coated PS spheres show intensity fluctuation under an optical microscope due to their Brownian rotational motion. Immobilized particles on the surface of the particle or the solid substrate limit this rotation restraining the intensity fluctuation. By analyzing the angular distribution of the particle, it becomes possible to investigate weak interactions between the unlabeled molecules with the data of time-dependent rotational angle derived from the fluorescent intensity. This study shows the convenience of the Janus-type materials for both chemical and biological sensors.

In addition, Dai *et al.* demonstrated a very remarkable study based on an ethanol-aged SnO_2 film gas sensor, in which an operating temperature-modulated reversible gas sensing transition for Sarin was developed.[30] The mechanism is based on the oxidation and reduction capabilities of Sarin gas at different temperatures (see Fig. 2). At 300 °C, Sarin behaves as an oxidizing gas causing the SnO_2 film gas sensor showing an abnormal sensing response with increased resistance; at other temperatures, Sarin shows a typical reductive gas property with decreasing resistance. In addition to Sarin detection, these Janus redox switches are also able to identify the specified gas in the presence of other reductive gases, such as DMMP, EtOH, and acetone.

B. Stabilizers

The applicability of Janus particles (JPs) as stabilizers for emulsions is more advantageous compared to conventional surfactants and stabilizers due to the self-organization ability of Janus particles at the interface.[31–34] Schröder *et al.* presented a study for interfacial stabilization by soft Janus nanoparticles.[31] In this study, the stabilization of water with various interfaces such as oil, air, and solids by Janus particles comprising two hemispheres of polystyrene (PS) and poly(methacrylic acid) (PMMA) was investigated. The outcome of their study showed that besides their being effective on many systems, the prepared Janus particles were not suitable for stabilization of air, very hydrophobic oils, and pigments containing systems. Then, Lan *et al.* examined another system of Janus particles for emulsion stabilization by varying the configurations of the Janus particles.[32] The system consists of a homologous series of pH-responsive LPS/P(S-co-tBA)-n Janus particles synthesized via seeded emulsion polymerization. The stabilizing efficiency of the Janus particles was analyzed by tuning the pH. The concept of Janus structure parameter (JSP) was introduced to the description of the ratio of hydrophilic domain to the total particle. It was found out that JSP has an ignorable effect on the determination of emulsion types in case the water affinity of the two regions of a Janus particle is weak, whereas JSP has a significant effect on

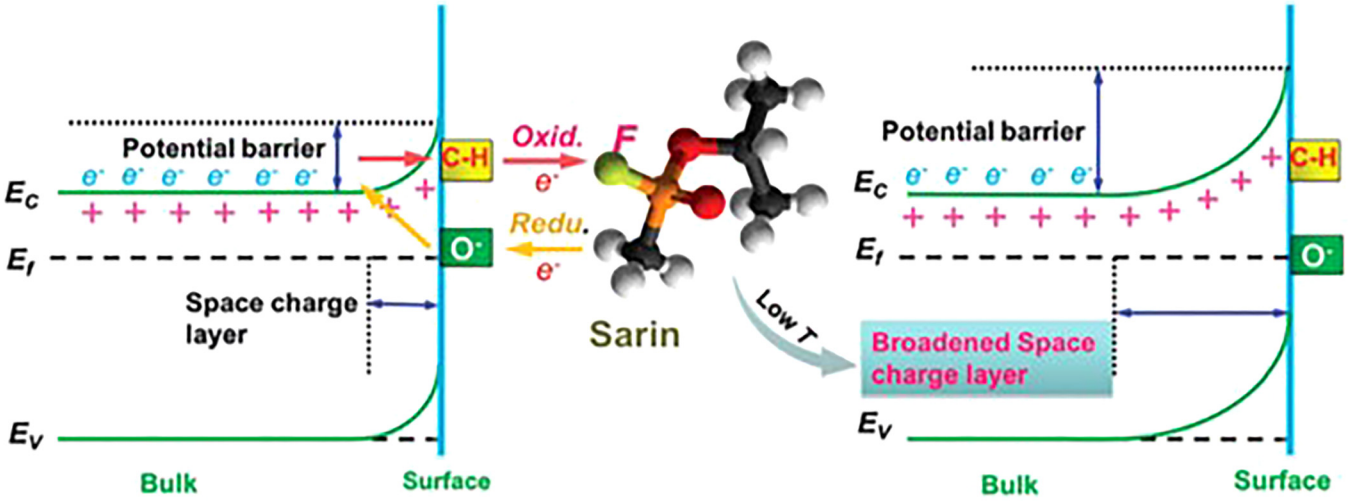

FIG. 2. Schematic illustration of the abnormal sensing mechanism for Sarin at 300 °C of the EtOH-aged SnO_2 sensor. Reproduced with permission from Dai *et al.*, Chem. Commun. **51**, 8193 (2015). Copyright 2015 Royal Society of Chemistry.

regulating the emulsion types when water affinity of the hydrophilic region of a Janus particle is strong.

Although it has been reported that the usage of Janus materials has many advantages;[31–34] recent studies[35,36] showed that the application of Janus materials for stabilizing purposes still needs further development. Razavi *et al.* discovered that chemically modified Janus particles were needed to be modified as their contributions to the systems at air/water interfaces were suppressed due to nanoscale capillary immersion forces in their study in which both chemically modified and physically modified Janus particles at the air/water interface were investigated.[35] In addition, Paiva *et al.* presented a model to investigate the effect of Janus particles on interfacial slip by applying a tangential shear flow at a planar polymer–polymer interface.[36] It was found out that long polymer grafts are needed to improve Janus particles as stabilizers; besides that, block copolymers have better stabilizing abilities compared to the Janus particles in spite of lower interfacial tension provided by Janus particles as reported previously by other scientists.[37,38]

C. Magnetism

Electrically or magnetically switchable Janus particles enable one to control the orientation of the particles under an external field giving rise to color formation, which makes these switchable Janus particles suitable for display applications.[12] In the study conducted by Yin *et al.*,[39] bifunctional magnetic-fluorescent responsive Janus supraballs were presented. For this purpose, first poly(methyl methacrylate-co-2-hydroxyethyl methacrylate)/cadmium acrylate ionomers [poly(MMA-co-HEMA)/Cd(AA) 2] with thermal stability and mechanical strength as the main ingredients of supraballs and poly(MMA-co-HEMA)/CdS QD-polymer hybrids were designed. Then by using microfluidic processing, Janus particles with excellent fluorescent and magnetoresponsive capabilities were prepared. The prepared two-faced Janus particles were templated on an epoxy resin to form a display (see Fig. 3) and the display was tested both under daylight and UV irradiation. On the basis of Janus-based display technologies, this study shows that Janus materials are good candidates as alternatives to the other techniques utilized for displays.

The study of Yin *et al.*[39] on the availability of Janus particles for display applications was followed by the study of Komazaki *et al.*, in which Janus-based handwriting-enabled display was achieved.[40] The Janus system forms both electrically and magnetically switchable twisting ball display, which is applicable to e-writers and electronic whiteboards (see Fig. 4).

As a pioneering study for the usage of Janus technology in quantum dots (QDs), Fan *et al.* revealed a study on the synthesis of Janus ZnO/Au nanocomposites (Au NP) and investigated the optical properties of the synthesized Janus nanocomposites.[41] The synthesis method was based on a bridge linking of 3-mercaptopropionic acid (3MPA) between ZnO QD (~4 nm) and Au NP (~6 nm). The defect emission was suppressed as the localized surface plasmon resonance (LSPR) peak of Au NPs matched with the defect emission of ZnO QDs resulting in a LSPR-assisted electron transfer process from Au NPs to ZnO QDs, which was proven by the time-resolved photoluminescence.

It was observed that Au NP incorporated ZnO QD showed a significant enhancement of UV emission and quenching visible emission compared to bare ZnO QDs with a decrease in the visible range emission intensity of ZnO/Au nanocomposites. This outcome was the proof of the mechanism of LSPR-enhanced UV-range emission of ZnO QDs, and it is also important for the improvement of the designing proper metal–semiconductor nanostructures with high luminescent efficiencies.

Other earliest examples of the usage of Janus technology for QDs were reported by Zhang *et al.* in which a synthetic pathway

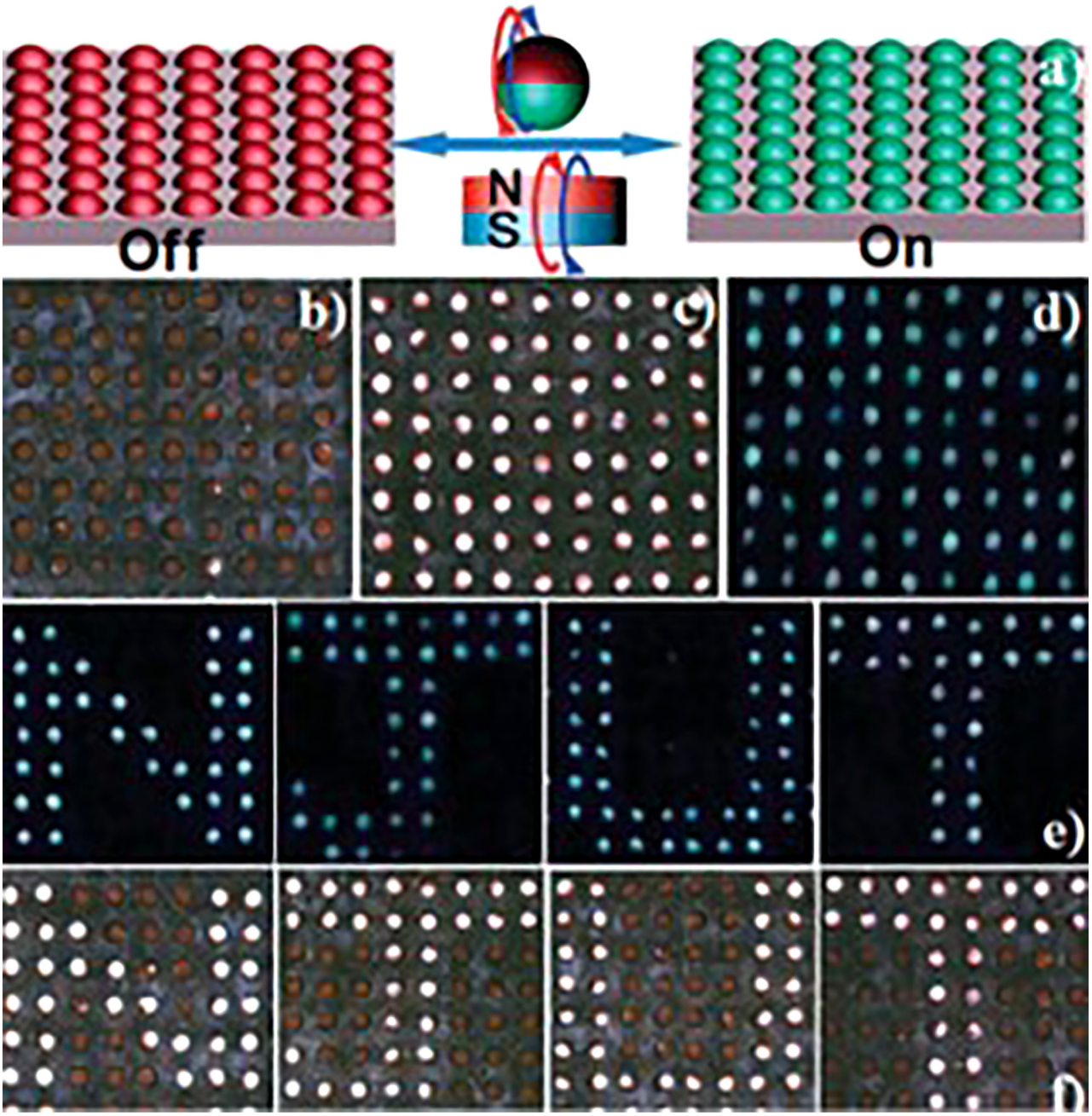

FIG. 3. (a) Schematic representation of a fluorescent switch of Janus particles controlled by varying the direction of an external magnetic field. [(b)–(f)] Optical images of the magnetoresponsive bead display prepared from Janus particles: [(b), (c), and (f)] under daylight and [(d) and (e)] under UV irradiation. Reproduced with permission from Yin *et al.*, Adv. Mater. **23**, 2915 (2011). Copyright 2011 Wiley-VCH.

for high-quality quantum dots was offered.[42] Cd/Pb chalcogenide heterostructured Janus particles were produced via the controllable cation exchange method. With thermally activated cation exchange, high-quality Pb-chalcogenide quantum dots were produced by the exchange of Cd^{2+} ions for Pb^{2+} cation. In addition to Cd^{2+}, it was observed that Zn^{2+} was also suitable for Pb^{2+} exchange. This method was developed to convert CdE, ZnO QDs to PbE where E = S, Se, or Te. It was observed that the size of the synthesized

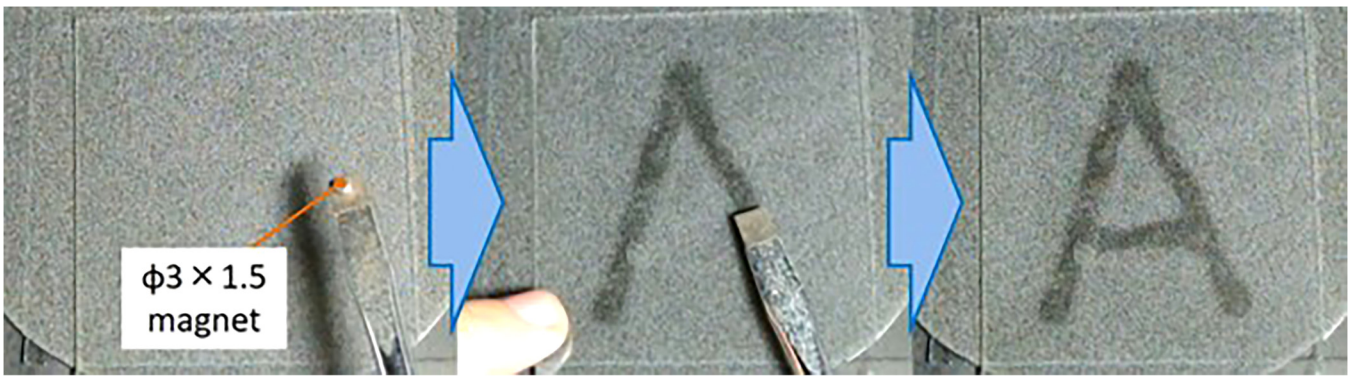

FIG. 4. Magnetic handwriting with a ø3 × 1.5 mm magnet with no voltage. Reproduced with permission from Komazaki *et al.*, J. Appl. Phys. **117**, 154506 (2015). AIP Publishing LLC.

PbE QDs lies in a large range. The sizes of the starting QDs were needed to be less than 6 and 5 nm for CdS and CdSe, respectively, for a complete cation exchange reaction. However, it was also possible to perform cation exchange with larger QDs in the presence of additional precursor.

The prepared heterostructures based on Pb showed interesting optoelectronic properties, which enable this system to be applicable on various areas. In addition to being applicable on other hot injection and heating-up systems, this approach promises for QD solar cells. With improved air stability and higher power conversion efficiencies, which are 6.2% for PbSe[15] and 7.2% for PbS[17], these heterostructures are promising structures for the enhancement of solar cell efficiencies through harnessing multiple excitation generation compared to QD-based solar cells fabricated from the standard procedure by using PbO.

The improvement of the device performance of quantum dot light-emitting diodes (QLEDs) with ligand asymmetric Janus QDs was achieved by Cho *et al.*[43] For this sake, blue QLEDs were incorporated with QDs with asymmetrically modified ligands, dodecylamine on top, and poly(amidoamine) dendrimer generation 0 at the bottom. The top layer provides uniform deposition of organic hole transport layers with enhanced hole injection properties, besides the bottom layer which is in contact with the ZnO electron transport layer works as a robust adhesive layer and an effective electron blocking layer (see Fig. 5).

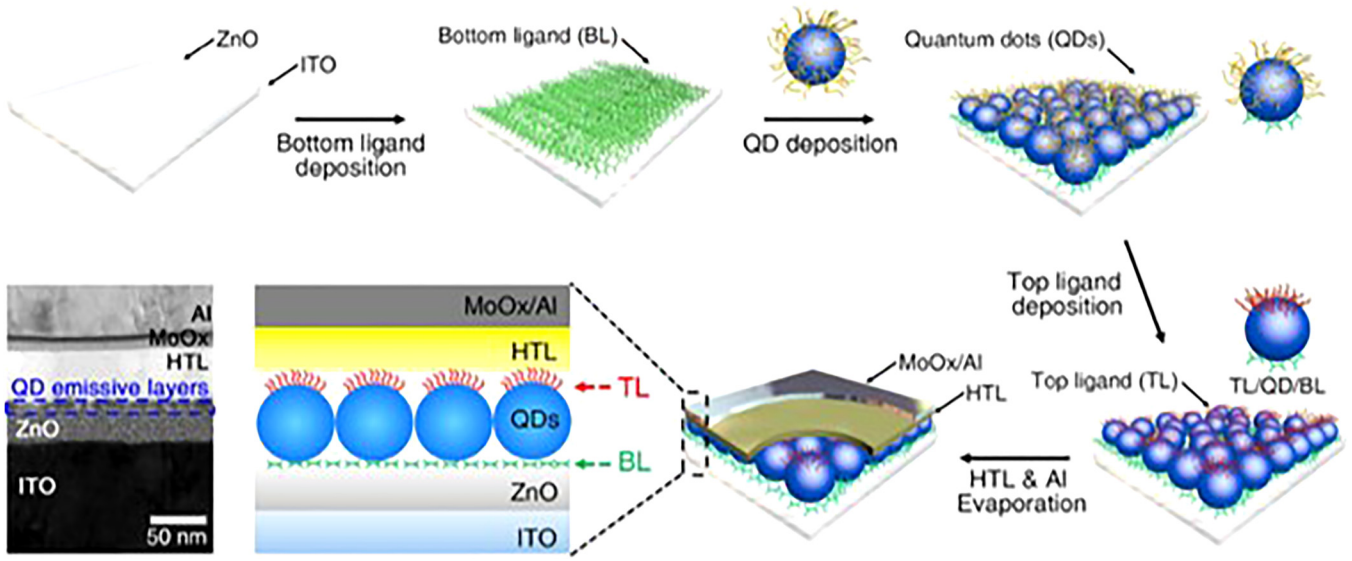

FIG. 5. Schematic illustration of the fabrication process for blue QLED incorporating ligand-asymmetric Janus QDs and its cross-sectional TEM image. Reproduced with permission from Cho *et al.*, ACS Appl. Mater. Interfaces **10**, 22453 (2018). Copyright 2018 American Chemical Society.

The peak external quantum efficiency of the blue QLED adopting ligand asymmetric QD displays (peak EQE = 3.23%) was calculated as more than twice the peak external quantum efficiency of the QDs with native ligands (peak EQE = 1.49%), oleic acid. This study demonstrates that ligand engineering allows the enhancement of the device performance of blue QLEDs which is also promising to understand QDs incorporated white light-emitting devices.

A new method on obtaining Janus quantum dot vesicles through membrane fusion was revealed by Li *et al.*[44] Driven by the inter-vesicular host–guest molecular recognition, the fusion of β-cyclodextrin (CD) or adamantane (Ada)-functionalized hyperbranched polymer vesicles incorporated with QDs ends up with the Janus vesicles. The giant size, great stability, and controllable surface functionality of the hyperbranched polymer vesicles enabled us to observe the vesicle structure and membrane fusion process with fluorescence microscopy (see Fig. 6), which introduces a new mechanism for the formation of Janus vesicles through a membrane fusion process. Prepared Janus vesicles show uniqueness compared to previously published ones due to three reasons: the formation mechanism, the structure of the vesicles, and the presence of two different QD hemispheres, which emit photoluminescence of two distinct colors upon excitation. This achievement was the first printing of ordered vesicles by incorporating a

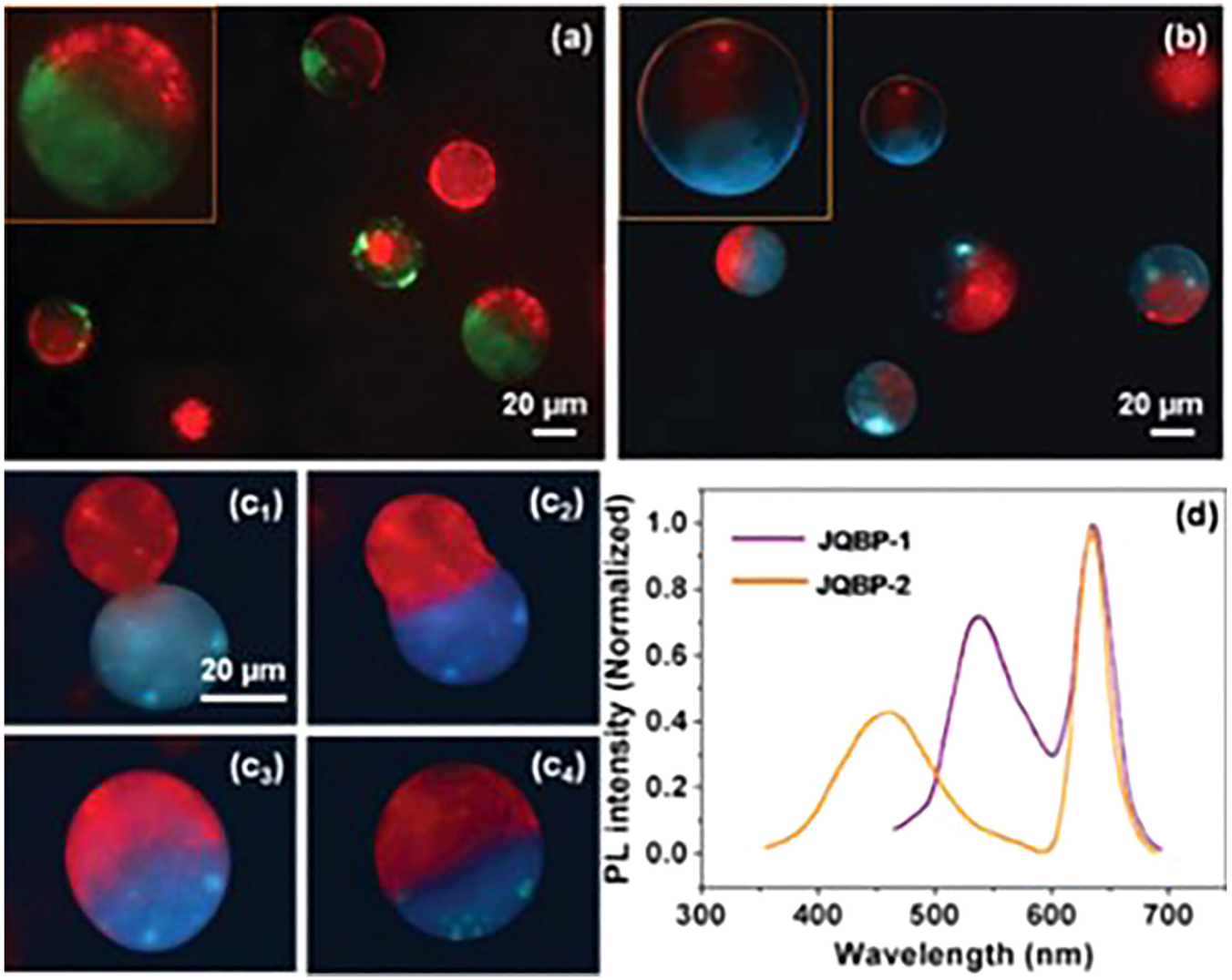

FIG. 6. Fluorescence micrographs of Janus QD vesicles: (a) JQBP-1 and (b) JQBP-2. (c) Real-time vesicle fusion process of QBP-1 and QBP-3 tracked under a fluorescent microscope. (c1) 0 s; (c2) 30 s; (c3) 100 s; (c4) 105 s. (d) PL spectra of JQBP-1 and JQBP-2 in aqueous solutions. Reproduced with permission from Li *et al.*, Mater. Chem. Front. **2**, 1040 (2018). Copyright 2018 Royal Society of Chemistry.

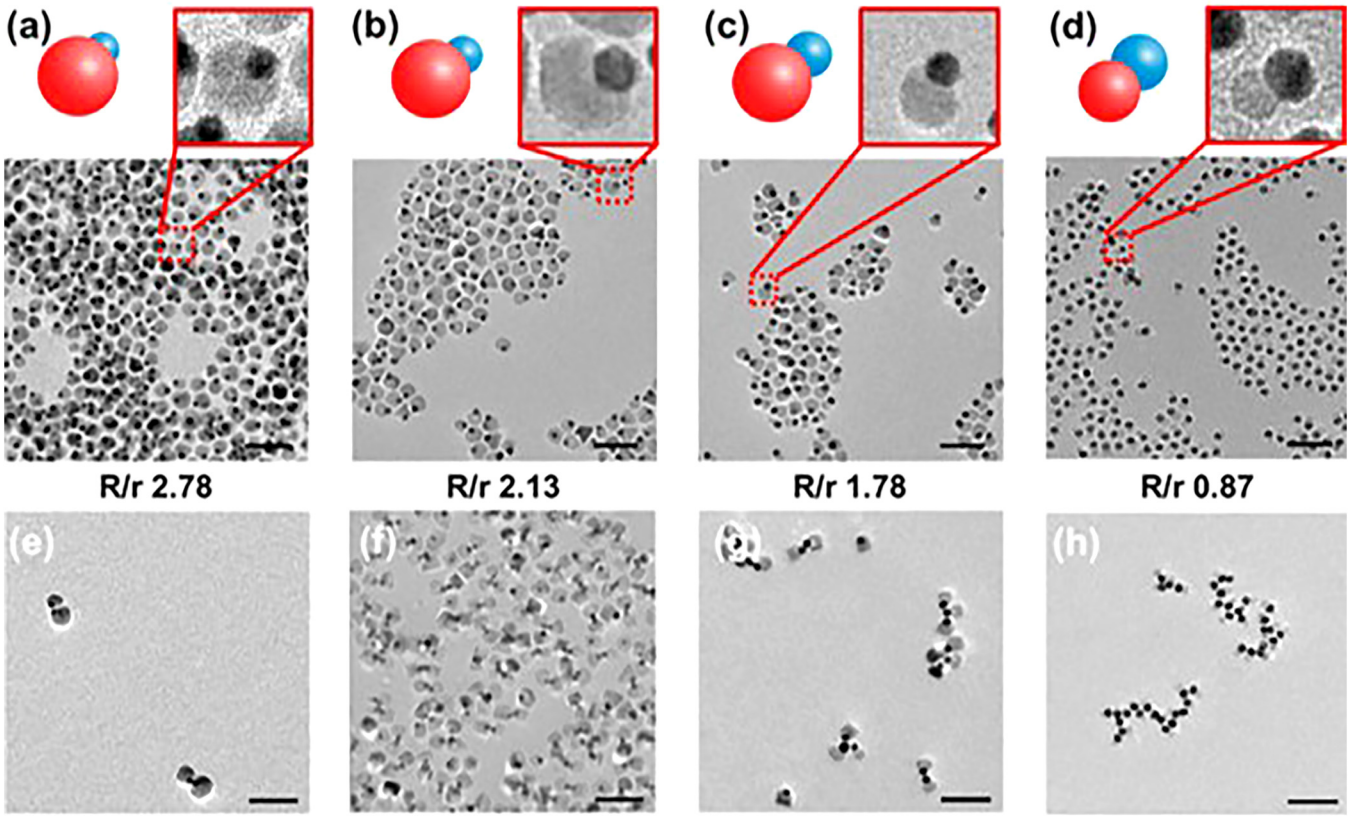

FIG. 7. Au–Fe_3O_4 dumbbell nanocrystals with different lobe size ratios in (a–d) organic solvent and (e–h) aqueous solutions correspondingly (all scale bars are 50 nm). Reproduced with permission from Liu *et al.*, Nano Lett. **19**, 1587 (2019). Copyright 2019 American Chemical Society.

Fe_3O_4-containing hemisphere into the Janus QD vesicles, which is a potential controlled printing application of Janus vesicles.

A controllable system of the self-assembly of Janus dumbbell nanocrystals in aqueous solutions by balancing the hydrophobic and hydrophilic moieties was developed by Liu *et al.*[45] To do that, Janus Au-Fe_3O_4 dumbbell nanocrystals (~20 nm) with the hydrophobic ligand coated Au lobe and negatively charged hydrophilic ligand coated Fe_3O_4 lobe were synthesized. To obtain different structures like clusters, chains, vesicles, and capsules, the lobe size ratio (see Fig. 7), surface coating, external conditions, and additional growth of Au nanocrystal domains on the Au lobe of dumbbell nanoparticles (Au-Au-Fe_3O_4) were systematically adjusted. It was observed that, being pH sensitive, the self-assembly of Janus dumbbell nanocrystals can be controlled reversibly.

Au lobe attraction and Fe_3O_4 lobe repulsion are balanced by assembly structures due to the fact that the asymmetric modification of these dumbbell nanostructures allows directional interactions between individual nanoparticles. Prepared series of assemblies showed that the hydrophobic Au lobes preferred to gather. Being directly correlated with the Au coupling, these superstructures exhibited different levels of enhanced surface plasmon resonance. Unique Au-Au-Fe_3O_4 nanocrystals, assembled into capsule like superstructures, showed a stronger and broader LSPR band extending into the near-infrared region in the presence of larger structures formed by Au-Au-Fe_3O_4 assembly. These assembly structures may lead to improving the magnetic and surface plasmonic properties, which could be used for the enhancement of applications including sensing, disease diagnoses, and therapy.

Recently, Nam *et al.* investigated photonic Janus balls with controlled magnetic moment and density asymmetry by making two compartments, a photonic compartment and a black compartment, from Janus balls consisting of two photocurable resins having different densities.[46] The photonic compartment, heavy resin, is composed of monodisperse silica particles in a monomer of ethoxylated trimethylolpropane triacrylate (ETPTA) containing photoinitiator; and the black compartment, light resin, is composed of carbon black nanoparticles and barium ferrite ($BaFe_{12}O_{19}$) nanoparticles in a photocurable silicone precursor. The paired drops spontaneously align vertically under the action of gravity due to the density mismatch, and magnetic nanoparticles are aligned with the help of an external field applied during photopolymerization. This phenomenon resulted in simultaneously switching of the orientation and structural color (see Fig. 8) by having two distinct

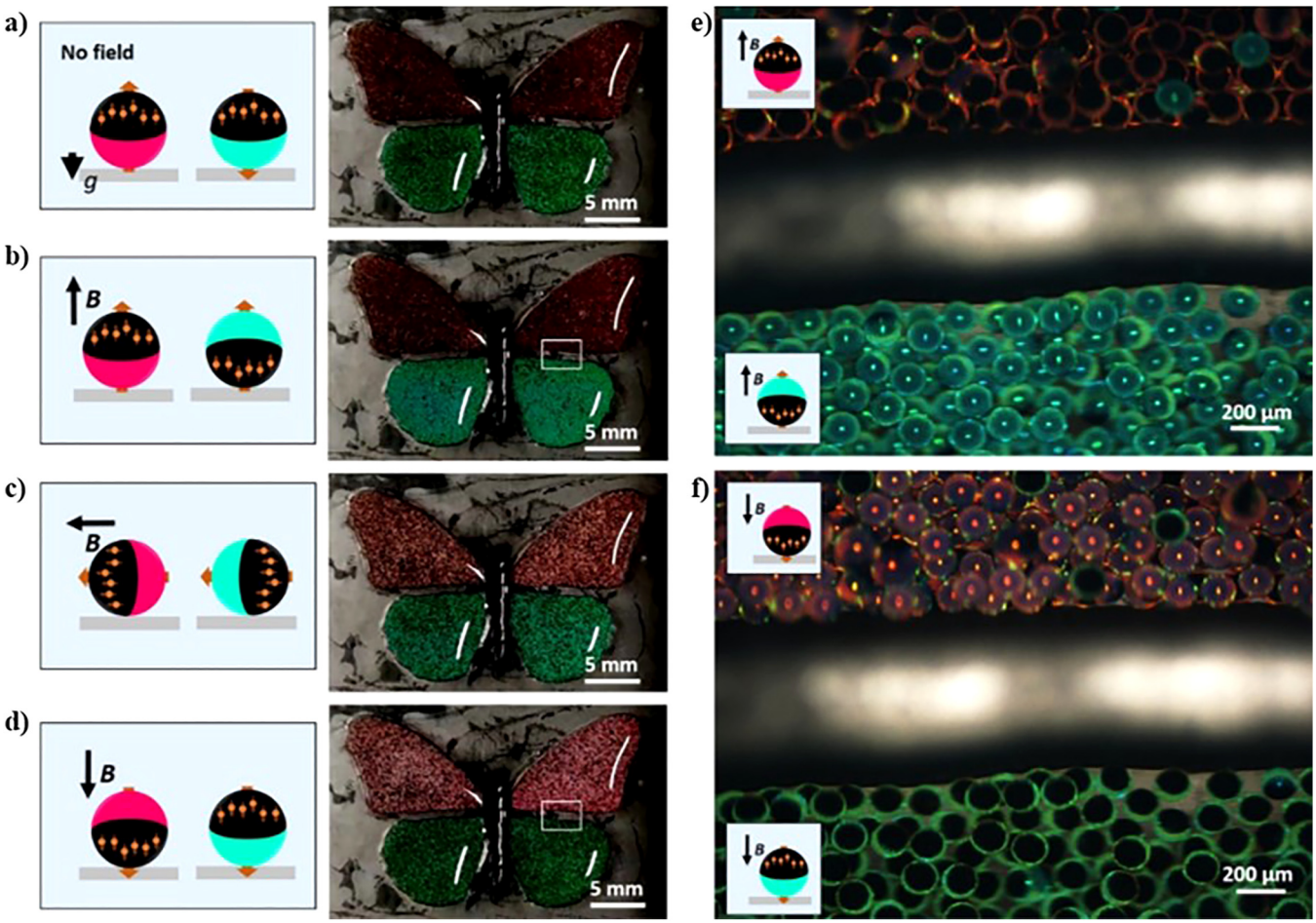

FIG. 8. Regioselective structural color switching. (a–d) Sets of schematic and optical image showing a regioselective color switching in a butterfly pattern, under four different field conditions, whose top wings contain red Janus balls with the upward magnetic moment and bottom wings contain green Janus balls with the downward magnetic moment. Bottom wings become green under the downward field (b), whereas top wings become red under the upward field (d). Both wings show a muted color without field (a), which become red and green at relatively low brightness under the parallel field to the substrate (c). (e, f) OM images taken at the boundary between the top and bottom wings under upward (e) and downward (f) field. Porous photonic compartments show brighter colors than composite ones.

photonic Janus balls with opposite directions of magnetic moment as it allows to set the direction of the magnetic moment relative to the axis of Janus balls in a programmed manner. These novel magneto responsive Janus materials have a great potential to be used for anti-counterfeiting tags as active color inks.

D. Surface modification

The first example of the application of Janus materials for the modification of textile surfaces was reported in Synytska and co-workers` study[47] in which water-repellent textile was achieved by immobilizing amphiphilic micrometer and submicrometer sized Janus particles on the hydrophilic textile surface. As the first step, polyethylene terephthalate (PET) fabric was modified with poly (glycidyl methacrylate) (PGMA) in order to take the advantage of reactive epoxy groups. Partial functionalization of Si particles with aminopropyl-trimethoxy silane (APS) to obtain reactive amine sides was followed by the adsorption of octadecyltrichlorosilane (OTS) on the unoccupied side of the particles. The reaction between the amine groups of Janus particles with the epoxy groups on the textile leads to the hydrophobic side (OTS modified) of the Janus particles to face the environment. It was also observed that the efficiency of the textile surfaces depends on the size of the particles as smaller particles (200 nm) are deposited on the fibers while larger particles (1 mm) are deposited between the fibers resulting in relatively poor hydrophobicity.

In order to investigate the mechanical properties of the JP modified surface in comparison to the surface modified with commercially available TiO_2 NPs, TiO_2-SiO_2 JPs were synthesized via Pickering emulsion method and applied on cotton fabric by Panwar

et al.[48] JP-treated cotton fabric was found to be mechanically stronger than TiO_2 NP-treated cotton fabric. It was observed that JP-treated cotton fabric maintains its mechanical durability even after long periods of UV exposure. In another JP-based study for surface modification, Ag-SiO_2 Janus particles with varying functionalities, i.e., amine, thiol, and epoxy on the exposed surface of SiO_2, were synthesized and their antimicrobial activity was investigated.[49] Prepared isotropic AgNPs and functionalized Ag-SiO_2 Janus particles were attached on cotton fabric for antimicrobial testing. It was observed that Ag-SiO_2 Janus particles showed better antimicrobial activity and high durability to washing compared to AgNPs.

E. Photocatalytic applications

The necessity for the improvement of the materials suitable for photocatalytic applications has arisen from the inefficient catalytic performance of TiO_2, which is the most used material in photocatalytic applications in the literature.[50,51] The necessary step to improve the catalytic performance of TiO_2 was taken by Pradhan *et al.*,[52] in which an efficient method for the oxidation of methanol by Janus nanostructures based on Au-TiO_2 heterodimers was presented. For this purpose, the preparation of Janus gold nanoparticles via interfacial ligand exchange reactions was followed by the growth of TiO_2 nanoparticles on the hydrophilic side of Janus gold nanoparticles. The prepared Au-TiO_2 snowman-like nanostructures were tested for their photocatalytic performance by the reaction of methanol into formaldehyde.

As another photocatalytic application, Co_2O_3-C_3N_4-Pt bifunctional hollow carbon nitride nanospheres (HCNS) were synthesized via template assisted growth followed by wet deposition by Zheng *et al.* to promote water splitting by photoredox catalysis.[53] The modification of HCNS brought separated oxidation and reduction centers at their nanodomains, which results in enhanced photocatalytic activity. In addition to enhanced photocatalytic activity, prevention of undesired reverse reaction of water and decrease in charge recombination also took place with the Janus-type modification of HCNS.

Au/CdSe Janus nanoparticles were synthesized by Liu *et al.* in order to improve photocatalytic hydrogen generation.[54] As the dependence of the performance of the metal–semiconductor heterostructures is related not only with morphology, but also with the interface between two counterparts, the performance of Au/CdSe Janus particles was expected to be significantly higher than CdSe half-shells grown on the Au nanospheres. For the synthesis of Au/CdSe Janus nanoparticles, the initial step was to prepare stabilized Au nanoparticles via seeded-mediated growth method. Then, three steps, Ag wetting layers deposition, Ag selenization, and CdSe selective growth, were followed to obtain Au/CdSe Janus nanospheres with a flat and high-quality interface. Prepared Au/CdSe Janus particles were then tested to investigate the efficiency of their photocatalytic activity, and it was reported that the photocatalytic hydrogen generation of the prepared Au/CdSe Janus particles was found to be 3.9 times higher than CdSe half-shells overgrown on the Au nanospheres.

F. Environmental applications

Organic pollutants, such as pesticides, phenolic compounds, nitrogen-containing compounds, and phthalates, are serious problems to be solved as it is as dangerous as heavy metal contamination for the nature. Photocatalytic reactions could be an effective option for the degradation of organic compounds, which may occur via various mechanisms like industrial wastewater, agriculture, or domestic effluents.[55] Fu *et al.* showed a simple approach based on an array of gold-titania Janus nanoparticles for the photocatalytic degradation of methylene blue, which is often called as model pollutant.[56] In order to do that, the mixture of polystyrene-block-poly (ethylene oxide) (PS-b-PEO)/$HAuCl_4$ solution and titania sol–gel precursor solution was spin coated. Then, organic matrix was removed by deep UV irradiation and arrays of Au-TiO_2 Janus-like nanoparticles obtained from $HAuCl_4$ and titania, which are previously incorporated in the PEO domains. In addition to its simplicity, Au-TiO_2 heterointerfaces of the Janus nanoparticles brought an enhanced photocatalytic activity compared to the bare TiO_2 or Au-TiO_2 composite nanoparticles.

Besides organic pollutants, inorganic pollutants also cause irreversible damages to the nature. For instance, lead contamination is a very crucial problem as it threatens living bodies in water and the land by being a poisonous heavy metal. A safe and a practical solution, which is based on the preparation of novel Janus-compartmental alginate microbeads for the selective colorimetric detection and efficient removal at the same time of Pb(II), was offered by Kang *et al.*[57] The aforementioned Janus microbeads have two divided phases of sensory polydiacetylene (PDA) liposomes and magnetic nanoparticles; alginate matrix is used here as an absorbent. In addition to successful detection and the removal of Pb(II), this system ensures enhanced sensitivity, fast detection without any change in colorimetric property, and stability of the microbeads in time due to the applied magnetic field (see Fig. 9).

It was reported that streptavidin-modified retroreflective JPs were found to be suitable for the selective and sensitive optical detection of Hg^{2+} ions with a detection limit of 0.027 nm by Chun *et al.*[58] Recently, Wang *et al.* introduced a facile microfluidic fabrication technique in order to obtain hybrid Au nanorod@Ag polyaniline Janus nanoparticles as a surface-enhanced Raman scattering sensor for Hg^{2+} ions.[59] The detection limit of the sensor was found to be linearly dependent on the Hg^{2+} concentration.

In addition to heavy metal contamination, the pollutants from the fuels also threaten the nature severely. To overcome this issue, fossil fuels are being taken into consideration. However, high costs and environmentally risky techniques used for the recovery of the oils bring the necessity of improvement in the techniques in order to benefit fossil fuels safely. Although silicon and metal oxide-based nanoparticles are suitable to be used for this purpose, they provide low efficiency due to their missing amphiphilicity.[55] As a solution to this issue, a promising system build up with graphene-based Janus amphiphilic nanosheets with a very low concentration of 0.01 wt. % for the recovery of tertiary or enhanced oil recovery was presented by Luo *et al.*[60] With the accumulation of these nanosheets at the oil–water interface, interfacial tension in a saline medium is reduced. Then, the separation of oil and water phases occurs with the climbing of solid-like interfacial film. The efficiency of the Janus nanosheets here was calculated as 15.2%. Right after this study, the same group continued with the same system with lower concentrations of nanosheets targeting to save huge amounts of saved water and recovered oil.[61] With the concentration of

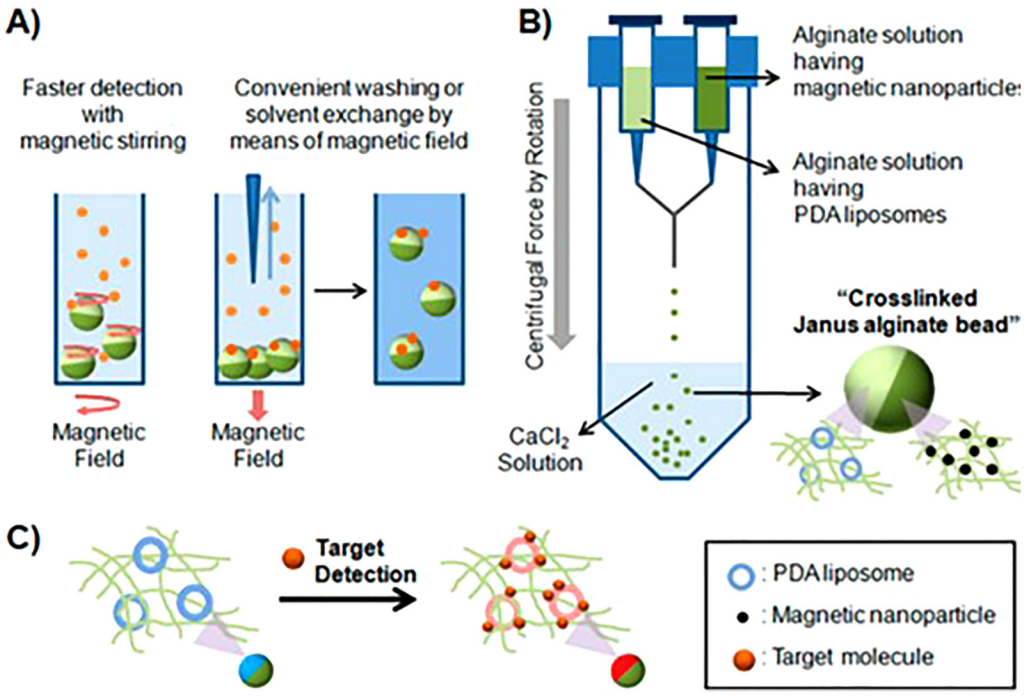

FIG. 9. (a) Janus magnetic microbeads provide fast and convenient handling and detection of target molecules in homogeneous solutions. (b) Schematic illustration of the fabrication procedure of the Janus-compartmental microbeads having sensory PDA liposomes and magnetic nanoparticles. (c) Colorimetric detection of target lead(II) Ions by the Janus magnetic microbeads. Reproduced with permission from Kang *et al.*, ACS Appl. Mater. Interfaces **6**, 10631 (2014). Copyright 2014 American Chemical Society.

0.005 wt. % nanosheets, the efficiency values raised up to 7.5%. Compared to the former study, efficiency seems halved; on the other hand, with a lower nanosheet concentration, saving higher amounts of water and oil, which could assure very effective techniques applicable to industry, was successfully achieved.

III. BIO-APPLICATIONS OF JANUS MATERIALS

The innovations in biological science have been crucial for the sake of new methods and materials to understand living life and to develop new methods for diagnosis and treatment for humans and animals. Having the potential to be multifunctional and mobile, Janus materials have taken place among new biological nanotechnology studies, especially in targeted systems. Although most of the studies on the bio-applications of Janus materials are based on drug delivery and imaging systems,[62] these novel materials have also been used for understanding cellular functions and tissue engineering.

A. Drug delivery

As the common methods, especially the ones used for cancer treatment, result in damages to healthy parts of the body by applying to the whole body instead of diseased parts; noninvasive, target oriented methods are essential for drug delivery. Usage of nanoparticles could be one option for drug delivery; however, it is difficult to locate different drugs on a single nanocarrier due to the different physicochemical properties of drugs.[63] By having more than one chemical function in a single unit, Janus particles offer a unique potential for disease treatment compared to nanoparticles as they have the potential to comprise different drugs at the same time in addition to be mobile.[64–66] To achieve targeted drug delivery, polystyrene/Fe_3O_4@SiO_2, a superparamagnetic Janus nanocomposite, was synthesized by Wang *et al.*[67] using sol–gel and miniemulsion methods and it was followed by the conjugation of folic acid on polystyrene and chemical adhesion of doxorubicin drug to the silica surface. Multimodal imaging opportunity was seen to be provided with Fe_3O_4 nanoparticles proving the potential of Janus particles to perform active targeting, drug delivery, and imaging simultaneously (see Fig. 10).[67] As another example, nanostructure incorporated Janus cages were prepared by Chen *et al.*[68] These Janus cages, which can be modified with smart polymers, showed the functionality of Janus particles by allowing targeted therapy by holding and releasing guest molecules in and out of the nanopores. Among these, there are various studies on drug delivery and targeting with Janus materials, especially for cancer diagnosis and treatment in the literature.[69–72]

B. Diagnosis and treatment

In many diseases, early diagnosis is vital for a fast, efficient treatment process. High resolution imaging techniques are very

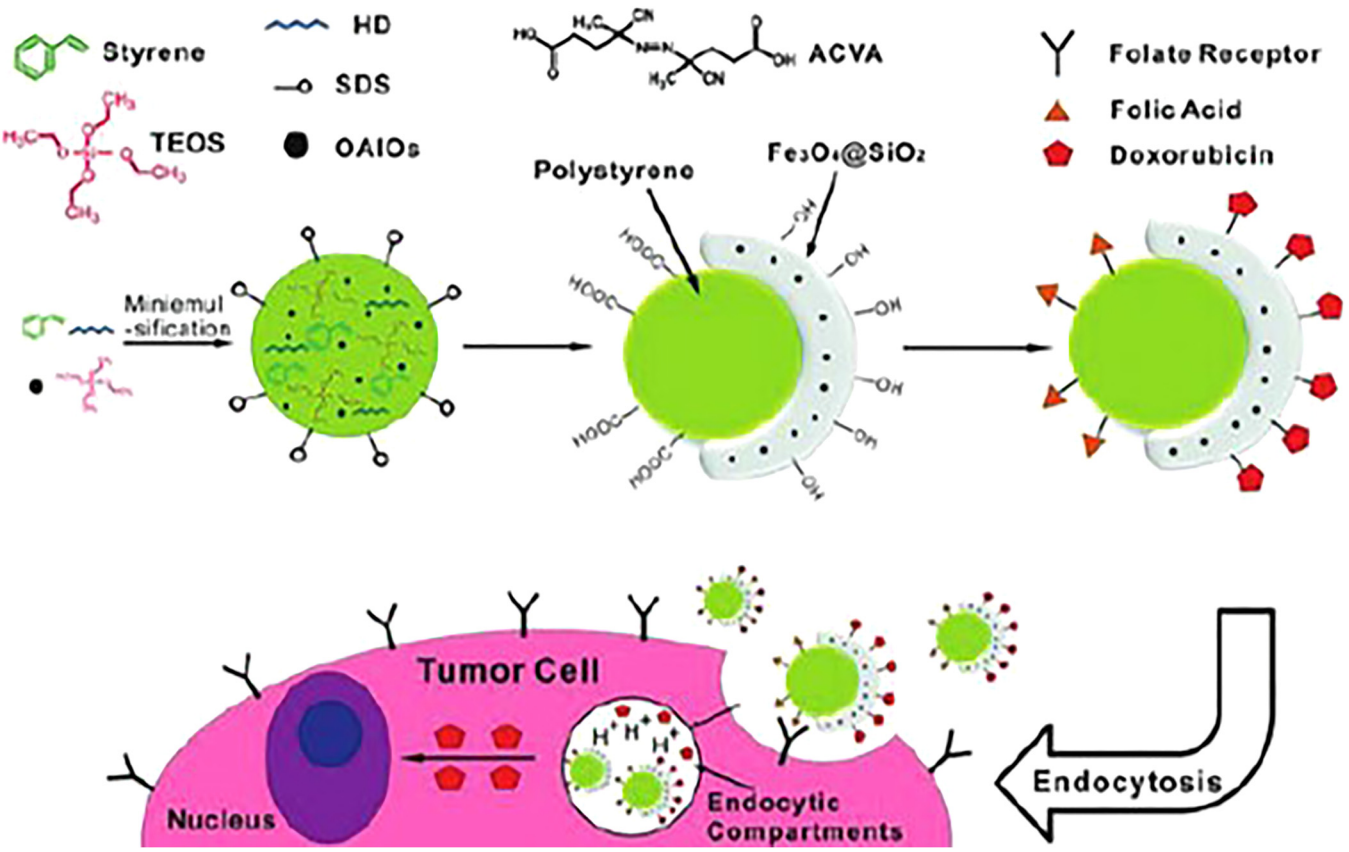

FIG. 10. Interaction of $Fe_3O_4@SiO_2$ Janus nanoparticle with tumor cell. Reproduced with permission from Wang *et al.*, Adv. Mater. **25**, 3485 (2013). Copyright 2013 Wiley-VCH.

important for the pre-detection and treatment of various pathologies. There are many noninvasive imaging methods with high spatial resolution [e.g., magnetic resonance imaging (MRI) and optical near-infrared (NIR)] However, these methods may be insufficient in parameters such as time delay in imaging and convenience.[73,74] Due to their adjustable multiple chemical functions in a single unit, Janus materials can provide multimodal imaging and eliminate the aforementioned problems as well.[74] In order to use in bio-imaging, multi-component gold-mesoporous silica, Janus nanoparticles were designed by Wang *et al.*[75] These multifunctional Janus nanostructures with folic acid were modified to target hepatocellular carcinoma (HCC). With the help of folic acid modification, a system serving as both targeted computed tomography (CT) and imaging agents for HCC diagnosis with Janus nanoparticles was achieved (see Fig. 11). On the other hand, gold-iron oxide-based Janus nanoprobes were reported in the study of Reguera *et al.*, in which the performance of Janus nanoprobes as contrast agents could be tuned by adjusting the Janus configuration.[76] Besides these examples mentioned here, Janus materials have proven themselves to be applicable for noninvasive bio-imaging studies.[77–79]

One of the main challenges of drug delivery and imaging is the presence of macrophages and neutrophils, which eliminate drug carriers before they reach the target site. Recent studies showed that Janus particles are good candidates to prevent the elimination of the drug by macrophages and neutrophils. For instance, by synthesizing two-sided structures of polyethylene glycol (PEG) chains and Janus particles coupled with immunoglobulin G(IgG), Sanchez *et al.* achieved to beat the issue of interferences.[80] Experimental results with macrophage cells showed that particles coated with only half PEG can escape from the immune system more effectively than particles coated with fully PEG.

Tissue engineering, which is another important window for the treatment of the illnesses lying with diagnosis and drug delivery, is based on using tissue scaffolds for healing and replacement of biological tissues. Today, studies involving nanoparticles are pretty common in tissue engineering, especially for tissue regeneration.[81,82] As an example of Janus materials in tissue engineering, strawberry-like silica JNPs with rough and smooth surfaces on the opposite sides comprise polymer containing spiropyran groups (PSP) and imidazoline groups for rough and smooth sides, respectively, were designed by Cao *et al.*[83] The ability of engineered

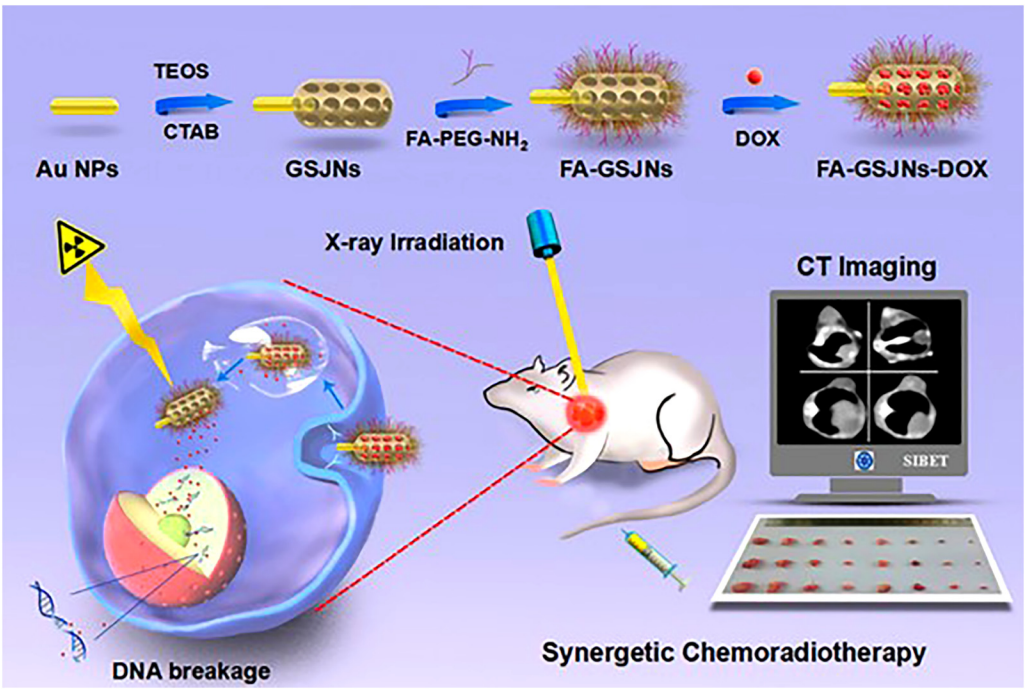

FIG. 11. Synthetic pathway of Janus nanoparticles and the usage of nanoparticles in CT imaging. Reproduced with permission from Wang *et al.*, ACS Nano **11**, 12732 (2017). Copyright 2017 American Chemical Society.

JNP-generated coatings to control cell–substrate interactions via irradiation allows the cells to be captured and released. Janus magnetic cellular spheroids with the spatial control of extracellular magnetic nanoparticles designed by Mattix *et al.* showed that magnetic NPs can be successfully incorporated into Janus spheroids while leaving the cell without damaging the cells. Moreover, it has been shown that with the presence of magnetic nanoparticles, complex tissues can be developed using magnetic force.[84]

IV. TOWARD ULTRATHIN 2D JANUS CRYSTALS

Thanks to considerable experience in chemistry and biology for the synthesis and targeted use of Janus-type materials, it has recently been possible to develop ultrafine 2D crystal forms of these materials. This section provides an up-to-date review and perspective on the synthesis and application areas of few-atom-thick two-dimensional materials. Ultrathin two-dimensional van der Waals (vdW) materials had drawn the attention of the scientific community following the announcement of single-layer (SL) form of graphite, namely, graphene, with its unique electronic, mechanical, and optical properties arising from the crystal symmetry.[85,86] Although graphene is a miraculous material, there is a great need for nanoscale materials with many different properties in different fields of developing nanotechnology. Therefore, obtaining Janus-type forms of ultrathin materials introduces a great variety of novel materials for nanoscale applications.

A. Graphene based Janus crystals

One of the studies that lead to the discovery of functionalized derivatives of graphene belongs to Sofo *et al.* who demonstrated that the saturation of delocalized electrons in π orbitals in graphene sheets opens a bandgap of 3.5 eV.[87] Later, the SL form of hydrogenated graphene, graphane, was experimentally realized by exposing the graphene to hydrogen atoms using cold plasma technique.[88] The one side hydrogenated graphene, namely, *graphone*, was predicted to be a ferromagnetic insulator, as the electrons in unsaturated π orbitals act as localized magnetic dipoles due to the restricted interaction between π-π bonds.[89] As a consequence of the asymmetric charge distribution resulting from the electronegativity difference between H and C atoms, the graphone was admitted to be the first 2D Janus material. The first experimental strategies on modifying the single side of graphene were mainly about the partial hydrogen covering to demonstrate a tunable bandgap by controlling the hydrogen coverage.[90–93] Repeated hydrogen patterns existing on one side of graphene sheet were obtained by the para-type chemisorption of H atoms that forms C_4H phase of hydrogenated graphene Janus crystal and displays comparably enhanced stability and wide bandgap within the UV range.[94]

Following the preliminary studies, graphene-based Janus structures have been extended by introducing halogen atoms. Li *et al.* successfully covered 8% of the basal plane of graphene by linking the chlorine atoms with the photochemical reaction that leads to transformation from sp^2 to sp^3 hybridization, which is related to

broken π bonds in C atoms, and the structural transformation opens bandgap in chlorinated graphene revealed by ultraviolet-visible absorption spectroscopy.[95] Later, possible scenarios for the mechanism of single-sided chlorine adsorption were investigated by Yang *et al.* and were found that the covalently bonded Cl phase is stable until the optimum coverage level reaches 25%, since the Cl_2 cluster formation is energetically feasible when much higher Cl levels are introduced to the system.[96]

Moreover, Robinson *et al.* synthesized the fluorinated Janus derivative of graphene that possesses C_4F composition with 25% coverage driven by highly reactive XeF_2 gas.[97] It was seen that the process enables the metal to insulator transition with a bandgap calculated to be 2.93 eV, indicating the suitability of fluorinated graphene for optoelectronic device applications. In addition, Singh and Bester demonstrated that the chair-like conformation of hydrofluorographene, in which either side of the carbon plane decorated by H and F atoms bonded on top of C atoms, is the dynamically stable ground state structure displaying a direct bandgap.[98] For the synthesis of novel asymmetric graphene derivatives, Zhang *et al.* demonstrated a unique technique that comprised of two-step functionalization. The fabrication starts with the one-sided functionalization of Si-supported graphene by the chemisorption of free halogen radicals using the photohalogenation process, then the halogenated layer was peeled off from the substrate by flexible poly (methyl methacrylate) to decorate the clean side with aryl/oxygen-functional groups (see Fig. 12). To indicate the effect of halogenated side on the reaction kinetics of the phenylation process, Raman spectroscopy was also utilized.[99]

B. Transition metal dichalcogenides

Another 2D material class that has been shown to be possible to obtain Janus-type forms is transition metal dichalcogenides (TMDs). 2D crystals of TMDs, where transition metal atoms are sandwiched between chalcogen atoms forming MX_2 composition (M = Mo, W while X = S, Se, Te), have been attracted for decades as being atomically thin quantum emitters.[100] The interest in their SL has continued over the past decade due to the promising electrical,[101] optical,[102,103] and physical properties,[104,105] making them suitable for future nanodevice applications. Recently, their Janus structures have been demonstrated, within the form of MXY (X and Y refer to different types of chalcogen atom), in which the mirror symmetry is broken due to the coverage of top and bottom atomic planes with different chalcogen atoms. Since each type of chalcogen atom possesses different electronegativity, the charge distribution on outer planes varies depending on the nonsymmetric arrangement, which leads to permanent dipole formation aligned through axial direction and causes Zeeman and Rashba spin splitting.[106–108] Moreover, theoretical approaches revealed that lack-of-symmetry in Janus TMDs unveils novel properties compared to traditional ones, such as vertical piezoelectricity,[109] enhanced catalytic activity,[110] and longer exciton lifetimes.[111]

The growth of the first Janus TMD, MoSSe, was demonstrated by the efforts of two different research groups. Zhang *et al.* realized the corresponding Janus structure reacting the as-grown $MoSe_2$ monolayer (on SiO_2/Si substrates) with vaporized sulfur that completely replaces the upper Se-layer with S atoms (see Fig. 13).[112] Conversely, Lu *et al.* broke the mirror symmetry in monolayer MoS_2 (on sapphire substrates) by first peeling the topmost S layer with H_2 plasma, then coating it with Se atoms using the thermal selenization process.[113] Apparently, it is seen that MoSSe is an optically active semiconductor and displays vertical piezoelectric response and second harmonic generation and also distinguishable from the pristine MoS_2 and its alloyed structures through the Raman spectroscopy. Recently, Lin *et al.* reported the transformation of suspended WS_2 monolayer to Janus WSSe by the use of laser pulse deposition technique that provides S to Se substitution for the topmost atomic layer within the suitable kinetic energy regime for Se atoms, which is ∼3–5 eV/atom at 300 °C.[114]

However, the theoretical predictions obtained prior to the expensive and time-consuming experimental studies also provide important information about the electronic, phononic, and optical characteristics of Janus-type 2D crystals. For example, using the first-principles calculations, Kandemir *et al.* showed that monitoring the effect of asymmetrical vertical strain on Janus-type single layers of MoSSe is possible via its vibrational spectrum. It was concluded that the vertical anisotropic feature of the Janus-type crystal can be utilized for the determination of detection of which side of the material interacts with the externals such as substrate, functional groups, or dopants.[115] It was also reported in another study that 2H phase of Janus-type WSSe SL corresponds to a stable structure. In addition, thanks to the vibrational characteristics, which stem from the distinctive interlayer interactions at different sides, the stability and stacking types of the bilayer of WSSe Janus structure can be monitored.[116] Moreover, the interlayer interactions within the vertical heterostructures of MoS_2 and MoSSe layers were reported to increase compared to the conventional ones because of the polarity in the Janus structure.[117] The strong interaction can be monitored through the Raman data obtained from the shear and breathing phonon modes. Further, Li *et al.* explained the physical mechanism of Janus WSSe and MoSSe under applied pressure, by means of diamond anvil cell, by examining the evolution of vibrational and optical properties with Raman and photoluminescent (PL) spectroscopy.[118] According to their results, the structures were found to be durable to high pressures (∼15 GPa) and the compressive strain causes a blueshift in PL peak.

C. Group-III monochalcogenides

Group III monochalcogenides, with the formula MX (M = Al, Ga, In; X = S, Se, Te), are 2D hexagonal semiconductor crystals that display a direct bandgap in their bulk form, which lies in the range of visible to near-infrared regime depending on the atomic composition.[119–122] 2D tetralayered slabs are comprised of the successive vertical arrangement of chalcogen–metal–metal–chalcogen atomic layers, in which chalcogen atoms are trigonally coordinated to axially aligned metal atoms. In the MX crystal system, dimensional reduction causes a direct to indirect bandgap transition[123] and offers many unique electronic and optical properties revealed by experimental and theoretical studies.[124–128]

Janus-type forms of Group-III monochalcogenides are one of the most studied ultrathin graphene-like materials nowadays. One

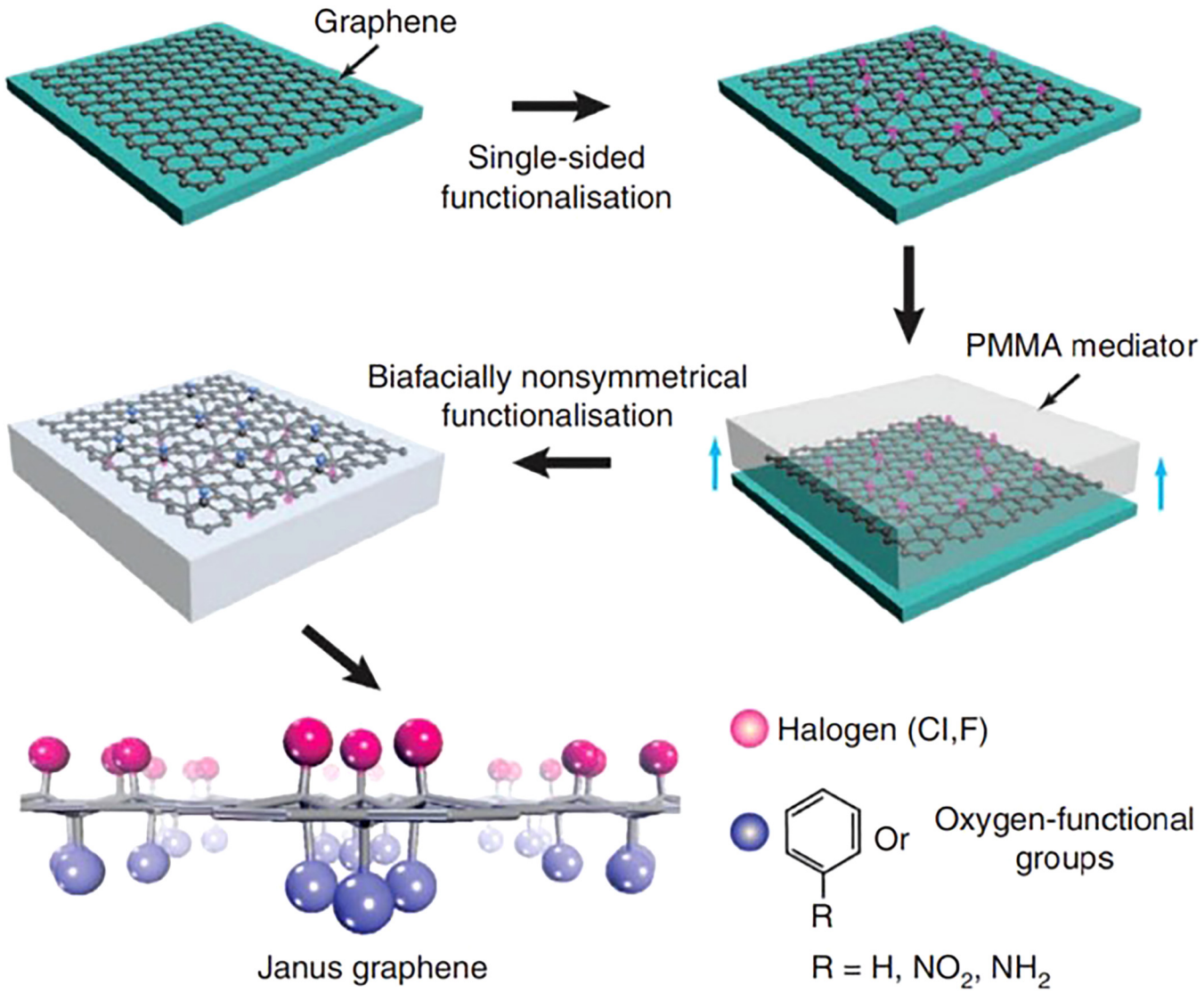

FIG. 12. Schematic representation of the fabrication process of two-sided functionalized graphene by the utilization of poly(methyl methacrylate) (PMMA) as an assistance substrate. Reproduced with permission from Zhang *et al.*, Nat. Commun. **4**, 1443 (2013). Copyright 2013 Nature Research.

of the earliest studies was based on the Janus SL structure of In_2SSe, which is a dynamically stable direct bandgap semiconductor, in contrast to its analogs, indirect bandgap semiconductors InS and InSe SL.[129] Nevertheless, the electronic structure of the Janus structure is durable against the compressive or tensile strain applied to the crystal structure. Following this, another study expanded the family by considering the various Janus structures having the formula of M_2XX' and $MM'X_2$ ($M/M' = In, Ga$, $X/X' = S, Se, Te$ and $M \neq M'$ and $X \neq X'$).[130] These dynamically stable semiconductors as free-standing SL crystals displayed reduced energy gaps and enhanced in-plane piezoelectric constants compared to that of pristine counterparts. Enhancement in piezoelectricity is related to a greater change in polarization under the applied strain. Because of the lack of inversion symmetry, Janus SL possesses out-of-plane piezoelectricity, which is found to be higher in $MM'X_2$ systems. Besides, only M_2STe and M_2SeTe structures possess a direct bandgap. In Ga_2XX' derivatives, Ga_2STe exhibits the lowest thermal conductivity over the considered temperature range, as it has a greater phonon scattering rate compared to Ga_2SeTe, even though they have similar phonon group velocities.[131] Moreover, Janus SL in the form of $MM'XX'$ (X and X′ can be the same type of atom) was found to be applicable for photocatalytic applications due to the suitability of bandgaps (lies within the visible range) and energy levels of the corresponding band edges.[132] In addition,

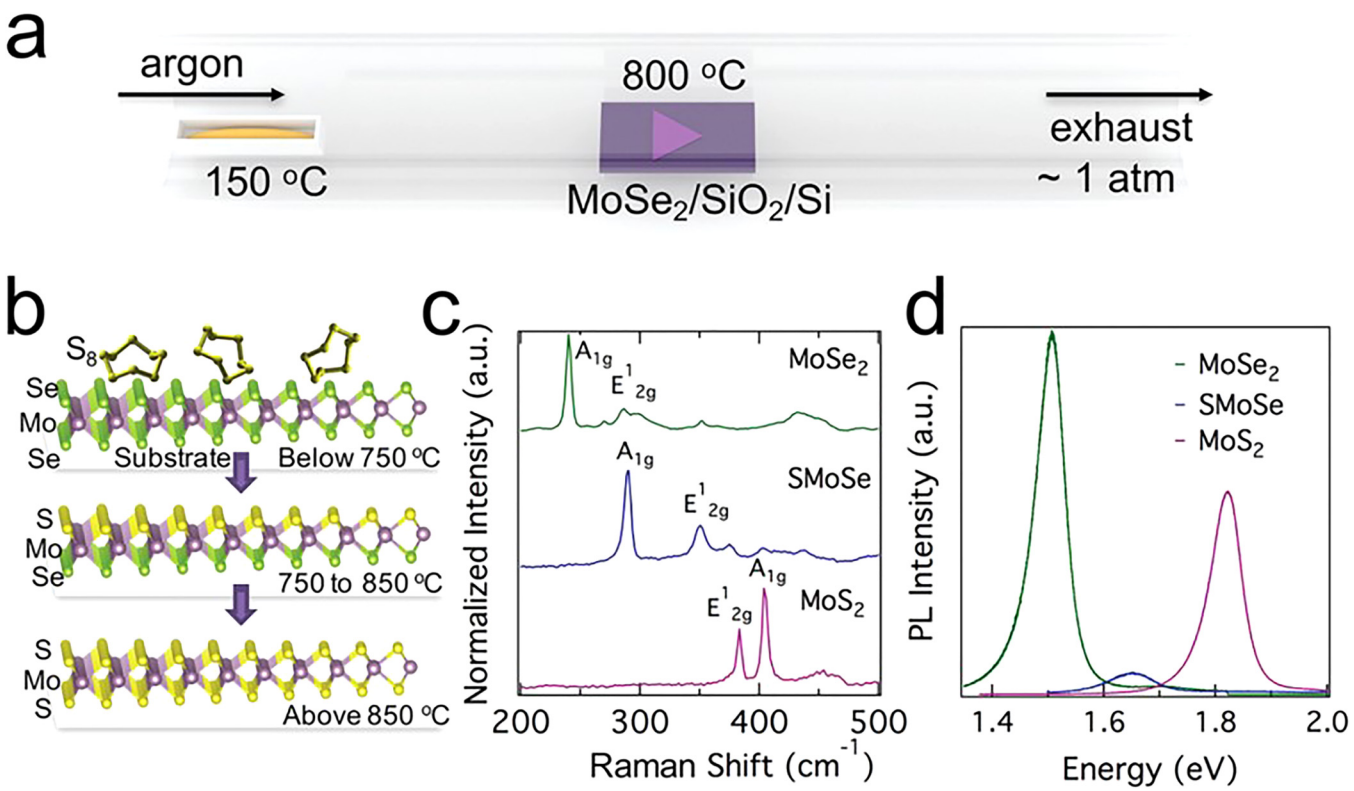

FIG. 13. (a) Schematic illustration for the growth process of monolayer $MoSe_2$ flakes. (b) The effect of temperature on selective sulfurization of SiO_2/Si supported monolayer $MoSe_2$. [(c) and (d)] The evolution of vibrational and optical characteristics of Janus and conventional TMDs by the use of Raman and PL spectroscopy. Reproduced with permission from Zhang *et al.*, ACS Nano **11**, 8192 (2017). Copyright 2017 American Chemical Society.

strain-based bandgap modification tailors the corresponding crystals to be used in water splitting applications. The oxygenated analogs with the chemical formula of Ga_2XO (X = S, Se, Te) were also added to the library of 2D Janus structures employing first-principle calculations.[133] Contrary to Ga_2SO and Ga_2SeO, Ga_2OTe is dynamically unstable, since the existence of the O atom weakens bonding between Ga-Te pairs. It was seen that Janus-type GaX crystals with O atoms induce indirect to direct bandgap transformation, which is controllable by the application of tensile or compressive strain. Further, these crystals are reported as optically active strong absorbers that reveal the suitability to be used in light-based device applications.

D. Bismuth tellurohalides

Bismuth tellurohalide, BiTeX (X = Cl, Br, I), structures can be attributed to the first examples of 2D Janus materials of which synthesis and structural properties were first reported in 1995.[134] These materials become distinctive from other 2D Janus materials previously mentioned above, as the crystal formation does not rely on any post-synthesis process, therefore can be introduced as "naturally occurring" van der Waals crystals within the 2D Janus family. The individual layers of polar BiTeX compounds that display hexagonal symmetry are composed of the trigonal coordination of Te and halide atoms around the central Bi atom. Each layer is separated by a van der Waals gap according to relatively weak interactions between the neighboring Te and X atoms. From the crystal family, BiTeCl was the first announced topological insulator that displays strong inversion asymmetry, confirmed by the utilization of angle-resolved photoemission spectroscopy (ARPES) measurements.[135] Several studies demonstrated the existence of the large Rashba effect in BiTeX crystals, which removes the degeneracy of energy states in opposite spins, as a consequence of the asymmetric crystal environment and strong spin–orbit interaction stems from Bi atoms.[136–139] In particular, optical excitations are allowed in BiTeX crystals, due to interband and intraband transitions in between Rashba type spin-splitted bands, approved by experimental and theoretical methods.[140–142] Such a relativistic electronic behavior with large spin splitting in 2D bulk systems implies the ability of material over their opponents to be integrated into device applications based on operating the spin degree of freedom like spintronics.[143,144] Earlier studies have focused extensively on the discovery of the physical environment of unique Janus systems over their bulk counterparts.[138,145,146]

Current research efforts have been in progress to obtain the low-dimensional structures and the corresponding properties of BiTeX crystals. Recently, Fülöp *et al.* discovered the Au-supported isolated SL of BiTeI by using stripped gold exfoliation technique.[147] To confirm the crystal formation and large surface area of SL BiTeI, scanning tunneling microscope and atomic force microscope measurements were utilized. The first-principles calculations revealed that the SL formation relies on the strong interaction between the Au-BiTeI interface that prevents the cleavage of contact SL from the Au surface during the exfoliation process. However, such an exfoliation process becomes incapable of producing large-scaled crystals that possess uniform sizes and high quality, in that case, the development of new techniques for the production is required. Hajra *et al.* overcame the problem through nanoconversion technique by exposing epitaxially formed Bi_2Te_3 to BiX_3 vapor to achieve ultrathin structures of BiTeX (<10 nm) that preserves high crystallinity (see Fig. 14).[148] This study is essential in terms of being a guidance for the production of low-dimensional Janus forms of different type 2D materials.

Furthermore, many theoretical approaches have been focused to clarify the low-dimensional characteristics of BiTeX crystals. Similar to their bulk counterparts, SL BiTeX structures are predicted to be topological insulators displaying polarity and large Rashba interaction.[149,150] In addition, Xiao *et al.* showed that BiTeI, as a free-standing SL, displays fascinating electronic, elastic, piezoelectric, mechanical, and electronic mobility properties.[151] As a result of large built-in potential owing to unbalanced charge distribution on outer planes, BiTeI presents higher out-of-plane piezoelectricity (0.556 pm/V) than the SL Janus structures of TMDs and group III monochalcogenides. Furthermore, it maintains dynamical stability and large Rashba interaction and possesses six times greater electronic mobility ($392\ cm^2\ V^{-1}\ s^{-1}$) compared to MoS_2. Predictions on thermoelectric properties of SL BiTeBr, implemented by combining the *ab initio* calculations and semiclassical Boltzmann transport theory, showed that the SL structure displays higher thermoelectric properties compared to that of the bulk structure, related to short phonon lifetimes that reduce the thermal conductivity.[152] In the case of n- or p-type doping, both bulk and SL crystals displayed enhanced thermoelectric properties according to greater ZT (figure of merit) values, which are found to be 0.55 and 0.75 for n- and p-type doping, respectively. Using the same methodology, it was shown that the thermoelectric properties of SL BiTeI demonstrate similar dependency to doping (ZT is 0.87 in p-type doping).[153] Its thermal conductance was found as

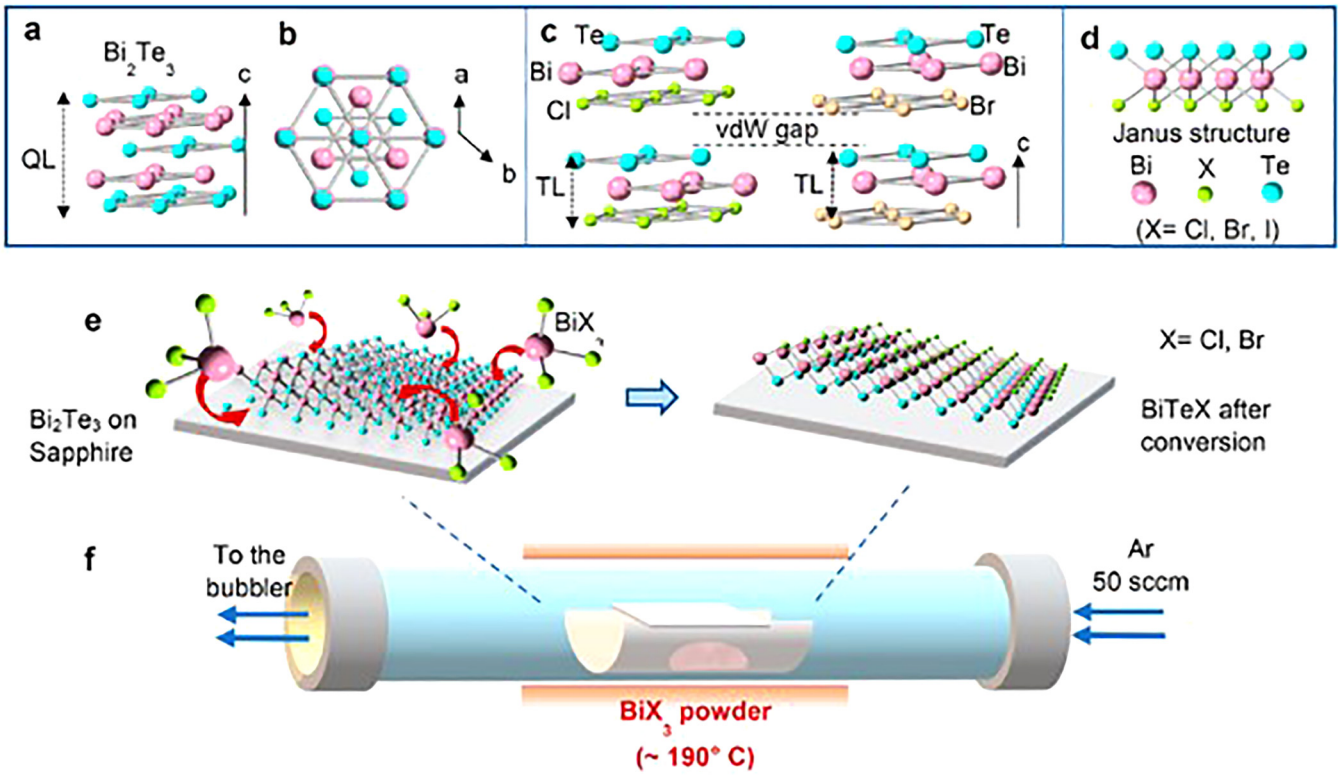

FIG. 14. [(a) and (b)] Top and side of one quintuple layer of Bi_2Te_3. (c) Anisotropic Janus structures of BiTeCl and BiTeBr. (d) Individual layer of the corresponding two-dimensional Janus BiTeX. (e) Atomic representation of Bi_2Te_3 to BiTeX transformation process and (f) the corresponding schematics of the experimental setup used for the nanoconversion process. Reproduced with permission from Hajra *et al.*, ACS Nano **14**, 15626 (2020). Copyright 2020 American Chemical Society.

12.6 W K^{-1}, which shows a lower value than that of SL crystals such as TMDs, group IV–VI, group-VA, and group-IV (except germanene) due to the small group velocity. In another study, the electronic properties of SL BiTeI were investigated under applied uniaxial strain, and it was concluded to be an efficient tool since broken symmetry in crystal alters the Rashba interaction by removing the isotropy in energy bands and induces the formation of the out-of-plane spin component.[154]

It is seen that the introduction of new ultrathin Janus-type crystals to the literature will not only expand the family of 2D crystals, but also lead to the emergence of nanoscale materials with brand new functions. Considering the requirements in devices operating at nanoscale, both experimental and theoretical studies on this material class would increasingly continue.

V. CONCLUSION

In this perspective, the story of the development of Janus-type materials over time and their applications that will appear in the near future are discussed. Janus-type materials, which first showed themselves in the field of chemistry, were used in fields such as sensing, catalysis, surface modification, separation, stabilizer, self-cleaning, nanoelectronics, electronic displays, and whiteboards. On the other hand, this material family has found a place in application areas such as detection, shuttle and transport of living cells, diagnosis, cellular therapy, and drug delivery in living organisms. In addition to the chemical and biological applications, current studies on Janus-type materials have mainly focused on the synthesis and understanding of ultrathin two-dimensional crystal structures. The discovery of this new material group, which is obtained by breaking the balance between surfaces of few-atom-thick crystals, is especially important in terms of nanotechnology, which will inevitably enter our lives in the near future.

ACKNOWLEDGMENTS

H.S. and Y.S. acknowledge financial support from the Scientific and Technological Research Council of Turkey (TUBITAK) under Project No. 117F095. H.S. acknowledges support from Türkiye Bilimler Akademisi-Turkish Academy of Sciences under the GEBIP program.

DATA AVAILABILITY

Data sharing is not applicable to this article as no new data were created or analyzed in this study.

REFERENCES

[1]A. Walther and A. H. E. Müller, Chem. Rev. **113**, 5194 (2013).
[2]J. Zhang, B. A. Grzybowski, and S. Granick, Langmuir **33**, 6964 (2017).
[3]H. Su, C.-A. Hurd Price, L. Jing, Q. Tian, J. Liu, and K. Qian, Mater. Today Bio **4**, 100033 (2019).
[4]G. Loget, J. Roche, and A. Kuhn, Adv. Mater. **24**, 5111 (2012).
[5]S. Granick, S. Jiang, and Q. Chen, Phys. Today **62**, 68 (2009).
[6]J. Zhang, E. Luijten, and S. Granick, Annu. Rev. Phys. Chem. **66**, 581 (2015).
[7]B. Liu, W. Zhang, D. Zhang, and X. Yang, J. Colloid Interface Sci. **385**, 34 (2012).
[8]J. Hu, S. Zhou, Y. Sun, X. Fang, and L. Wu, Chem. Soc. Rev. **41**, 4356 (2012).
[9]F. Wang, *Development of Janus Nanocomposites as a Multifunctional Nanocarrier for Cancer Therapy* (University of Cincinnati, 2013).
[10]J. Du and R. K. O'Reilly, Chem. Soc. Rev. **40**(5), 2402–2416 (2011).
[11]C. Kaewsaneha, P. Tangboriboonrat, D. Polpanich, M. Eissa, and A. Elaissari, Colloids Surf. A Physicochem. Eng. Asp. **439**, 35 (2013).
[12]E. Poggi and J. F. Gohy, Colloid Polym. Sci. **295**, 2083 (2017).
[13]M. Lattuada and T. A. Hatton, Nano Today **6**, 286 (2011).
[14]A. Perro, S. Reculusa, S. Ravaine, E. Bourgeat-Lami, and E. Duguet, J. Mater. Chem. **15**, 3745 (2005).
[15]C. H. Chen, R. K. Shah, A. R. Abate, and D. A. Weitz, Langmuir **25**, 4320 (2009).
[16]S. Yang, F. Guo, B. Kiraly, X. Mao, M. Lu, K. W. Leong, and T. J. Huang, Lab Chip **12**, 2097 (2012).
[17]A. C. Misra, S. Bhaskar, N. Clay, and J. Lahann, Adv. Mater. **24**, 3850 (2012).
[18]K. Roh, D. C. Martin, and J. Lahann, Nat. Mater. **4**, 759 (2005).
[19]G. Loget and A. Kuhn, J. Mater. Chem. **22**, 15457 (2012).
[20]N. Saito, Y. Kagari, and M. Okubo, Langmuir **23**, 5914 (2007).
[21]N. Saito, R. Nakatsuru, Y. Kagari, and M. Okubo, Langmuir **23**, 11506 (2007).
[22]F. S. Romanski, J. S. Winkler, R. C. Riccobene, and M. S. Tomassone, Langmuir **28**, 3756 (2012).
[23]D. Luo, F. Wang, B. V. Vu, J. Chen, J. Bao, D. Cai, R. C. Willson, and Z. Ren, Carbon **126**, 105 (2018).
[24]D. Luo, F. Zhang, H. Zheng, Z. Ren, L. Jiang, and Z. Ren, Chem. Commun. **55**, 1318 (2019).
[25]T. Cui, X. Li, B. Dong, X. Li, M. Guo, L. Wu, B. Li, and H. Li, Polymer **174**, 70 (2019).
[26]T. G. Roberts, J. N. Anker, and R. Kopelman, J. Magn. Magn. Mater. **293**, 715 (2005).
[27]S. Fournier-Bidoz, A. C. Arsenault, I. Manners, and G. A. Ozin, Chem. Commun. **28**, 441 (2005).
[28]W. F. Paxton, P. T. Baker, T. R. Kline, Y. Wang, T. E. Mallouk, and A. Sen, J. Am. Chem. Soc. **128**, 14881 (2006).
[29]J. Choi, Y. Zhao, D. Zhang, S. Chien, and Y. H. Lo, Nano Lett. **3**, 995 (2003).
[30]Z. Dai, G. Duan, Z. Cheng, L. Xu, T. Li, G. Liu, H. Zhang, Y. Li, and W. Cai, Chem. Commun. **51**, 8193 (2015).
[31]J. H. Schröder, M. Doroshenko, D. Pirner, M. E. J. Mauer, B. Förster, V. Boyko, B. Reck, K. J. Roschmann, A. H. E. Müller, and S. Förster, Polymer **106**, 208 (2016).
[32]Y. Lan, J. Choi, H. Li, Y. Jia, R. Huang, K. J. Stebe, and D. Lee, Ind. Eng. Chem. Res. **58**, 20961 (2019).
[33]Y. Song and S. Chen, Chem. Asian J. **9**, 418 (2014).
[34]B. P. Binks and P. D. I. Fletcher, Langmuir **17**(16), 4708–4710 (2001).
[35]S. Razavi, L. M. Hernandez, A. Read, W. L. Vargas, and I. Kretzschmar, J. Colloid Interface Sci. **558**, 95 (2020).
[36]F. L. Paiva, A. R. Secchi, V. Calado, J. Maia, and S. Khani, Soft Matter **16**, 6662 (2020).
[37]M. Borrell and L. G. Leal, Langmuir **23**, 12497 (2007).
[38]C. Vannozzi, Phys. Fluids **31**, 082112 (2019).
[39]S. N. Yin, C. F. Wang, Z. Y. Yu, J. Wang, S. S. Liu, and S. Chen, Adv. Mater. **23**, 2915 (2011).
[40]Y. Komazaki, H. Hirama, and T. Torii, J. Appl. Phys. **117**, 154506 (2015).
[41]X. Fan, C. Xu, X. Hao, Z. Tian, and Y. Lin, Europhys. Lett. **106**, 67001 (2014).
[42]J. Zhang, B. D. Chernomordik, R. W. Crisp, D. M. Kroupa, J. M. Luther, E. M. Miller, J. Gao, and M. C. Beard, ACS Nano **9**, 7151 (2015).
[43]I. Cho, H. Jung, B. G. Jeong, D. Hahm, J. H. Chang, T. Lee, K. Char, D. C. Lee, J. Lim, C. Lee, J. Cho, and W. K. Bae, ACS Appl. Mater. Interfaces **10**, 22453 (2018).
[44]H. Li, A. Zhang, K. Li, W. Huang, Y. Mai, Y. Zhou, and D. Yan, Mater. Chem. Front. **2**, 1040 (2018).
[45]F. Liu, S. Goyal, M. Forrester, T. Ma, K. Miller, Y. Mansoorieh, J. Henjum, L. Zhou, E. Cochran, and S. Jiang, Nano Lett. **19**, 1587 (2019).
[46]S. K. Nam, J. Bin Kim, S. H. Han, and S.-H. Kim, ACS Nano **14**, 15714 (2020).
[47]A. Synytska, R. Khanum, L. Ionov, C. Cherif, and C. Bellmann, ACS Appl. Mater. Interfaces **3**, 1216 (2011).

[48]K. Panwar, M. Jassal, and A. K. Agrawal, RSC Adv. **6**, 92754 (2016).
[49]K. Panwar, M. Jassal, and A. K. Agrawal, Carbohydr. Polym. **187**, 43 (2018).
[50]E. Arenas-Calderon, V. B. Medrano, and M. A. Guzmán, *Fundamentals of Nanoparticles* (Elsevier, 2018), pp. 51–70.
[51]P. D. Cozzoli, E. Fanizza, R. Comparelli, M. L. Curri, A. Agostiano, and D. Laub, J. Phys. Chem. B **108**, 9623 (2004).
[52]S. Pradhan, D. Ghosh, and S. Chen, ACS Appl. Mater. Interfaces **1**, 2060 (2009).
[53]D. Zheng, X. N. Cao, and X. Wang, Angew. Chem. Int. Ed. **55**, 11512 (2016).
[54]X.-D. Liu, K. Chen, S. Ma, Z.-H. Hao, S. Liang, L. Zhou, and Q.-Q. Wang, Nanoscale Res. Lett. **14**, 349 (2019).
[55]C. Marschelke, A. Fery, and A. Synytska, Colloid Polym. Sci. **298**, 841 (2020).
[56]X. Fu, J. Liu, H. Yang, J. Sun, X. Li, X. Zhang, and Y. Jia, Mater. Chem. Phys. **130**, 334 (2011).
[57]D. H. Kang, H. S. Jung, N. Ahn, S. M. Yang, S. Seo, K. Y. Suh, P. S. Chang, N. L. Jeon, J. Kim, and K. Kim, ACS Appl. Mater. Interfaces **6**, 10631 (2014).
[58]H. J. Chun, S. Kim, Y. D. Han, D. W. Kim, K. R. Kim, H.-S. Kim, J.-H. Kim, and H. C. Yoon, Biosens. Bioelectron. **104**, 138 (2018).
[59]Y. Wang, M. Shang, Y. Wang, and Z. Xu, Anal. Methods **11**, 3966 (2019).
[60]D. Luo, F. Wang, J. Zhu, F. Cao, Y. Liu, X. Li, R. C. Willson, Z. Yang, C. W. Chu, and Z. Ren, Proc. Natl. Acad. Sci. U.S.A. **113**, 7711 (2016).
[61]D. Luo, F. Wang, J. Zhu, L. Tang, Z. Zhu, J. Bao, R. C. Willson, Z. Yang, and Z. Ren, Ind. Eng. Chem. Res. **56**, 11125 (2017).
[62]G. Agrawal and R. Agrawal, ACS Appl. Nano Mater. **2**, 1738 (2019).
[63]L.-T.-C. Tran, S. Lesieur, and V. Faivre, Expert Opin. Drug Deliv. **11**, 1061 (2014).
[64]D. Shao, X. Zhang, W. Liu, F. Zhang, X. Zheng, P. Qiao, J. Li, W. Dong, and L. Chen, ACS Appl. Mater. Interfaces **8**, 4303 (2016).
[65]Y. Wu, X. Lin, Z. Wu, H. Möhwald, and Q. He, ACS Appl. Mater. Interfaces **6**, 10476 (2014).
[66]P. Sundararajan, J. Wang, L. A. Rosen, A. Procopio, and K. Rosenberg, Chem. Eng. Sci. **178**, 199 (2018).
[67]F. Wang, G. M. Pauletti, J. Wang, J. Zhang, R. C. Ewing, Y. Wang, and D. Shi, Adv. Mater. **25**, 3485 (2013).
[68]Y. Chen, H. Yang, C. Zhang, Q. Wang, X. Qu, J. Li, F. Liang, and Z. Yang, Macromolecules **46**, 4126 (2013).
[69]Z. Wang, Z. Chang, D. Shao, F. Zhang, F. Chen, L. Li, M. Ge, R. Hu, X. Zheng, Y. Wang, and W. Dong, ACS Appl. Mater. Interfaces **11**, 34755 (2019).
[70]S. Liang, X. Deng, Y. Chang, C. Sun, S. Shao, Z. Xie, X. Xiao, P. Ma, H. Zhang, Z. Cheng, and J. Lin, Nano Lett. **19**, 4134 (2019).
[71]A. Sánchez, K. Ovejero Paredes, J. Ruiz-Cabello, P. Martínez-Ruíz, J. M. Pingarrón, R. Villalonga, and M. Filice, ACS Appl. Mater. Interfaces **10**, 31032 (2018).
[72]X. Liu, M. Peng, G. Li, Y. Miao, H. Luo, G. Jing, Y. He, C. Zhang, F. Zhang, and H. Fan, Nano Lett. **19**, 4118 (2019).
[73]R. R. Raylman, S. Majewski, S. K. Lemieux, S. S. Velan, B. Kross, V. Popov, M. F. Smith, A. G. Weisenberger, C. Zorn, and G. D. Marano, Phys. Med. Biol. **51**, 6371 (2006).
[74]I. Schick, S. Lorenz, D. Gehrig, A.-M. Schilmann, H. Bauer, M. Panthöfer, K. Fischer, D. Strand, F. Laquai, and W. Tremel, J. Am. Chem. Soc. **136**, 2473 (2014).
[75]Z. Wang, D. Shao, Z. Chang, M. Lu, Y. Wang, J. Yue, D. Yang, M. Li, Q. Xu, and W. Dong, ACS Nano **11**, 12732 (2017).
[76]J. Reguera, D. Jiménez de Aberasturi, M. Henriksen-Lacey, J. Langer, A. Espinosa, B. Szczupak, C. Wilhelm, and L. M. Liz-Marzán, Nanoscale **9**, 9467 (2017).
[77]G. Song, X. Zheng, Y. Wang, X. Xia, S. Chu, and J. Rao, ACS Nano **13**, 7750 (2019).
[78]Y. Ju, H. Zhang, J. Yu, S. Tong, N. Tian, Z. Wang, X. Wang, X. Su, X. Chu, J. Lin, Y. Ding, G. Li, F. Sheng, and Y. Hou, ACS Nano **11**, 9239 (2017).
[79]F. Chen, M. Bai, Y. Zhao, K. Cao, X. Cao, and Y. Zhao, Anal. Chem. **90**, 2271 (2018).
[80]L. Sanchez, Y. Yi, and Y. Yu, Nanoscale **9**, 288 (2017).
[81]M. Yadid, R. Feiner, and T. Dvir, Nano Lett. **19**, 2198 (2019).
[82]S. Vial, R. L. Reis, and J. M. Oliveira, Curr. Opin. Solid State Mater. Sci. **21**, 92 (2017).
[83]Z. Cao, Q. Bian, Y. Chen, F. Liang, and G. Wang, ACS Macro Lett. **6**, 1124 (2017).
[84]B. M. Mattix, T. R. Olsen, M. Casco, L. Reese, J. T. Poole, J. Zhang, R. P. Visconti, A. Simionescu, D. T. Simionescu, and F. Alexis, Biomaterials **35**, 949 (2014).
[85]K. S. Novoselov, A. K. Geim, S. V. Morozov, D. Jiang, Y. Zhang, S. V. Dubonos, I. V. Grigorieva, and A. A. Firsov, Science **306**, 666 (2004).
[86]K. S. Novoselov, A. K. Geim, S. V. Morozov, D. Jiang, M. I. Katsnelson, I. V. Grigorieva, S. V. Dubonos, and A. A. Firsov, Nature **438**, 197 (2005).
[87]J. O. Sofo, A. S. Chaudhari, and G. D. Barber, Phys. Rev. B **75**, 153401 (2007).
[88]D. C. Elias, R. R. Nair, T. M. G. Mohiuddin, S. V. Morozov, P. Blake, M. P. Halsall, A. C. Ferrari, D. W. Boukhvalov, M. I. Katsnelson, A. K. Geim, and K. S. Novoselov, Science **323**, 610 (2009).
[89]J. Zhou, Q. Wang, Q. Sun, X. S. Chen, Y. Kawazoe, and P. Jena, Nano Lett. **9**, 3867 (2009).
[90]R. Balog, B. Jørgensen, L. Nilsson, M. Andersen, E. Rienks, M. Bianchi, M. Fanetti, E. Lægsgaard, A. Baraldi, S. Lizzit, Z. Sljivancanin, F. Besenbacher, B. Hammer, T. G. Pedersen, P. Hofmann, and L. Hornekær, Nat. Mater. **9**, 315 (2010).
[91]A. Bostwick, J. L. McChesney, K. V. Emtsev, T. Seyller, K. Horn, S. D. Kevan, and E. Rotenberg, Phys. Rev. Lett. **103**, 056404 (2009).
[92]D. Haberer, D. V. Vyalikh, S. Taioli, B. Dora, M. Farjam, J. Fink, D. Marchenko, T. Pichler, K. Ziegler, S. Simonucci, M. S. Dresselhaus, M. Knupfer, B. Büchner, and A. Grüneis, Nano Lett. **10**, 3360 (2010).
[93]D. Haberer, L. Petaccia, M. Farjam, S. Taioli, S. A. Jafari, A. Nefedov, W. Zhang, L. Calliari, G. Scarduelli, B. Dora, D. V. Vyalikh, T. Pichler, C. Wöll, D. Alfè, S. Simonucci, M. S. Dresselhaus, M. Knupfer, B. Büchner, and A. Grüneis, Phys. Rev. B **83**, 165433 (2011).
[94]D. Haberer, C. E. Giusca, Y. Wang, H. Sachdev, A. V. Fedorov, M. Farjam, S. A. Jafari, D. V. Vyalikh, D. Usachov, X. Liu, U. Treske, M. Grobosch, O. Vilkov, V. K. Adamchuk, S. Irle, S. R. P. Silva, M. Knupfer, B. Büchner, and A. Grüneis, Adv. Mater. **23**, 4497 (2011).
[95]B. Li, L. Zhou, D. Wu, H. Peng, K. Yan, Y. Zhou, and Z. Liu, ACS Nano **5**, 5957 (2011).
[96]M. Yang, L. Zhou, J. Wang, Z. Liu, and Z. Liu, J. Phys. Chem. C **116**, 844 (2012).
[97]J. T. Robinson, J. S. Burgess, C. E. Junkermeier, S. C. Badescu, T. L. Reinecke, F. K. Perkins, M. K. Zalalutdniov, J. W. Baldwin, J. C. Culbertson, P. E. Sheehan, and E. S. Snow, Nano Lett. **10**, 3001 (2010).
[98]R. Singh and G. Bester, Phys. Rev. B **84**, 155427 (2011).
[99]L. Zhang, J. Yu, M. Yang, Q. Xie, H. Peng, and Z. Liu, Nat. Commun. **4**, 1443 (2013).
[100]A. Splendiani, L. Sun, Y. Zhang, T. Li, J. Kim, C.-Y. Chim, G. Galli, and F. Wang, Nano Lett. **10**, 1271 (2010).
[101]B. Radisavljevic, A. Radenovic, J. Brivio, V. Giacometti, and A. Kis, Nat. Nanotechnol. **6**, 147 (2011).
[102]M. Bernardi, M. Palummo, and J. C. Grossman, Nano Lett. **13**, 3664 (2013).
[103]U. Wurstbauer, B. Miller, E. Parzinger, and A. W. Holleitner, J. Phys. D Appl. Phys. **50**, 173001 (2017).
[104]L. Cai, J. He, Q. Liu, T. Yao, L. Chen, W. Yan, F. Hu, Y. Jiang, Y. Zhao, T. Hu, Z. Sun, and S. Wei, J. Am. Chem. Soc. **137**, 2622 (2015).
[105]H. Zeng, J. Dai, W. Yao, D. Xiao, and X. Cui, Nat. Nanotechnol. **7**, 490 (2012).
[106]F. Li, W. Wei, H. Wang, B. Huang, Y. Dai, and T. Jacob, J. Phys. Chem. Lett. **10**, 559 (2019).
[107]M. Adhib Ulil Absor, H. Kotaka, F. Ishii, and M. Saito, Jpn. J. Appl. Phys. **57**, 04FP01 (2018).
[108]Y. C. Cheng, Z. Y. Zhu, M. Tahir, and U. Schwingenschlögl, Europhys. Lett. **102**, 57001 (2013).

[109]L. Dong, J. Lou, and V. B. Shenoy, ACS Nano **11**, 8242 (2017).
[110]D. Er, H. Ye, N. C. Frey, H. Kumar, J. Lou, and V. B. Shenoy, Nano Lett. **18**, 3943 (2018).
[111]H. Jin, T. Wang, Z.-R. Gong, C. Long, and Y. Dai, Nanoscale **10**, 19310 (2018).
[112]J. Zhang, S. Jia, I. Kholmanov, L. Dong, D. Er, W. Chen, H. Guo, Z. Jin, V. B. Shenoy, L. Shi, and J. Lou, ACS Nano **11**, 8192 (2017).
[113]A.-Y. Lu, H. Zhu, J. Xiao, C.-P. Chuu, Y. Han, M.-H. Chiu, C.-C. Cheng, C.-W. Yang, K.-H. Wei, Y. Yang, Y. Wang, D. Sokaras, D. Nordlund, P. Yang, D. A. Muller, M.-Y. Chou, X. Zhang, and L.-J. Li, Nat. Nanotechnol. **12**, 744 (2017).
[114]Y.-C. Lin, C. Liu, Y. Yu, E. Zarkadoula, M. Yoon, A. A. Puretzky, L. Liang, X. Kong, Y. Gu, A. Strasser, H. M. Meyer, M. Lorenz, M. F. Chisholm, I. N. Ivanov, C. M. Rouleau, G. Duscher, K. Xiao, and D. B. Geohegan, ACS Nano **14**, 3896 (2020).
[115]A. Kandemir, F. M. Peeters, and H. Sahin, J. Chem. Phys. **149**, 084707 (2018).
[116]A. Kandemir and H. Sahin, Phys. Chem. Chem. Phys. **20**, 17380 (2018).
[117]K. Zhang, Y. Guo, Q. Ji, A.-Y. Lu, C. Su, H. Wang, A. A. Puretzky, D. B. Geohegan, X. Qian, S. Fang, E. Kaxiras, J. Kong, and S. Huang, J. Am. Chem. Soc. **142**, 17499 (2020).
[118]H. Li, Y. Qin, B. Ko, D. B. Trivedi, D. Hajra, M. Y. Sayyad, L. Liu, S. Shim, H. Zhuang, and S. Tongay, Adv. Mater. **32**, 2002401 (2020).
[119]M. O. D. Camara, A. Mauger, and I. Devos, Phys. Rev. B **65**, 125206 (2002).
[120]V. Capozzi, Phys. Rev. B **23**, 836 (1981).
[121]M. Afzaal and P. O'Brien, J. Mater. Chem. **16**, 1597 (2006).
[122]N. C. Fernelius, Prog. Cryst. Growth Charact. Mater. **28**, 275 (1994).
[123]S. Demirci, N. Avazlı, E. Durgun, and S. Cahangirov, Phys. Rev. B **95**, 115409 (2017).
[124]D. A. Bandurin, A. V. Tyurnina, G. L. Yu, A. Mishchenko, V. Zólyomi, S. V. Morozov, R. K. Kumar, R. V. Gorbachev, Z. R. Kudrynskyi, S. Pezzini, Z. D. Kovalyuk, U. Zeitler, K. S. Novoselov, A. Patanè, L. Eaves, I. V. Grigorieva, V. I. Fal'ko, A. K. Geim, and Y. Cao, Nat. Nanotechnol. **12**, 223 (2017).
[125]S. Sucharitakul, N. J. Goble, U. R. Kumar, R. Sankar, Z. A. Bogorad, F.-C. Chou, Y.-T. Chen, and X. P. A. Gao, Nano Lett. **15**, 3815 (2015).
[126]P. Hu, Z. Wen, L. Wang, P. Tan, and K. Xiao, ACS Nano **6**, 5988 (2012).
[127]X. Zhou, J. Cheng, Y. Zhou, T. Cao, H. Hong, Z. Liao, S. Wu, H. Peng, K. Liu, and D. Yu, J. Am. Chem. Soc. **137**, 7994 (2015).
[128]G. Antonius, D. Y. Qiu, and S. G. Louie, Nano Lett. **18**, 1925 (2018).
[129]A. Kandemir and H. Sahin, Phys. Rev. B **97**, 155410 (2018).
[130]Y. Guo, S. Zhou, Y. Bai, and J. Zhao, Appl. Phys. Lett. **110**, 163102 (2017).
[131]Q. Zhong, Z. Dai, J. Liu, Y. Zhao, and S. Meng, Phys. E **115**, 113683 (2020).
[132]H. Yang, P. Zhao, Y. Ma, X. Lv, B. Huang, and Y. Dai, J. Phys. D Appl. Phys. **52**, 455303 (2019).
[133]M. Demirtas, B. Ozdemir, Y. Mogulkoc, and E. Durgun, Phys. Rev. B **101**, 075423 (2020).
[134]A. V. Shevelkov, E. V. Dikarev, R. V. Shpanchenko, and B. A. Popovkin, J. Solid State Chem. **114**, 379 (1995).
[135]Y. L. Chen, M. Kanou, Z. K. Liu, H. J. Zhang, J. A. Sobota, D. Leuenberger, S. K. Mo, B. Zhou, S.-L. Yang, P. S. Kirchmann, D. H. Lu, R. G. Moore, Z. Hussain, Z. X. Shen, X. L. Qi, and T. Sasagawa, Nat. Phys. **9**, 704 (2013).
[136]K. Ishizaka, M. S. Bahramy, H. Murakawa, M. Sakano, T. Shimojima, T. Sonobe, K. Koizumi, S. Shin, H. Miyahara, A. Kimura, K. Miyamoto, T. Okuda, H. Namatame, M. Taniguchi, R. Arita, N. Nagaosa, K. Kobayashi, Y. Murakami, R. Kumai, Y. Kaneko, Y. Onose, and Y. Tokura, Nat. Mater. **10**, 521 (2011).
[137]M. S. Bahramy, R. Arita, and N. Nagaosa, Phys. Rev. B **84**, 041202 (2011).
[138]S. V. Eremeev, I. A. Nechaev, Y. M. Koroteev, P. M. Echenique, and E. V. Chulkov, Phys. Rev. Lett. **108**, 246802 (2012).
[139]M. Sakano, M. S. Bahramy, A. Katayama, T. Shimojima, H. Murakawa, Y. Kaneko, W. Malaeb, S. Shin, K. Ono, H. Kumigashira, R. Arita, N. Nagaosa, H. Y. Hwang, Y. Tokura, and K. Ishizaka, Phys. Rev. Lett. **110**, 107204 (2013).
[140]J. S. Lee, G. A. H. Schober, M. S. Bahramy, H. Murakawa, Y. Onose, R. Arita, N. Nagaosa, and Y. Tokura, Phys. Rev. Lett. **107**, 117401 (2011).
[141]A. Akrap, J. Teyssier, A. Magrez, P. Bugnon, H. Berger, A. B. Kuzmenko, and D. van der Marel, Phys. Rev. B **90**, 035201 (2014).
[142]S. Schwalbe, R. Wirnata, R. Starke, G. A. H. Schober, and J. Kortus, Phys. Rev. B **94**, 205130 (2016).
[143]E. I. Rashba, Phys. Rev. B **86**, 125319 (2012).
[144]M. Sakano, J. Miyawaki, A. Chainani, Y. Takata, T. Sonobe, T. Shimojima, M. Oura, S. Shin, M. S. Bahramy, R. Arita, N. Nagaosa, H. Murakawa, Y. Kaneko, Y. Tokura, and K. Ishizaka, Phys. Rev. B **86**, 085204 (2012).
[145]A. Crepaldi, L. Moreschini, G. Autès, C. Tournier-Colletta, S. Moser, N. Virk, H. Berger, P. Bugnon, Y. J. Chang, K. Kern, A. Bostwick, E. Rotenberg, O. V. Yazyev, and M. Grioni, Phys. Rev. Lett. **109**, 096803 (2012).
[146]C. J. Butler, H.-H. Yang, J.-Y. Hong, S.-H. Hsu, R. Sankar, C.-I. Lu, H.-Y. Lu, K.-H. O. Yang, H.-W. Shiu, C.-H. Chen, C.-C. Kaun, G.-J. Shu, F.-C. Chou, and M.-T. Lin, Nat. Commun. **5**, 4066 (2014).
[147]B. Fülöp, Z. Tajkov, J. Pető, P. Kun, J. Koltai, L. Oroszlány, E. Tóvári, H. Murakawa, Y. Tokura, S. Bordács, L. Tapasztó, and S. Csonka, 2D Mater. **5**, 031013 (2018).
[148]D. Hajra, R. Sailus, M. Blei, K. Yumigeta, Y. Shen, and S. Tongay, ACS Nano **14**, 15626 (2020).
[149]Y. Ma, Y. Dai, W. Wei, X. Li, and B. Huang, Phys. Chem. Chem. Phys. **16**, 17603 (2014).
[150]D. C. Hvazdouski, M. S. Baranava, and V. R. Stempitsky, IOP Conf. Ser. Mater. Sci. Eng. **347**, 012017 (2018).
[151]W.-Z. Xiao, H.-J. Luo, and L. Xu, J. Phys. D Appl. Phys. **53**, 245301 (2020).
[152]S.-D. Guo and H.-C. Li, Comput. Mater. Sci. **139**, 361 (2017).
[153]S.-D. Guo, A.-X. Zhang, and H.-C. Li, Nanotechnology **28**, 445702 (2017).
[154]S.-H. Zhang and B.-G. Liu, Phys. Rev. B **100**, 165429 (2019).